Available online at www.sciencedirect.com

ScienceDirect

Geochimica et Cosmochimica Acta 313 (2021) 340–358

Geochimica et Cosmochimica Acta

www.elsevier.com/locate/gca

Deciphering the signatures of weathering and erosion processes and the effects of river management on Li isotopes in the subtropical Pearl River basin

Yilong Song [a], Xu (Yvon) Zhang [b,c], Julien Bouchez [b], Benjamin Chetelat [a,*], Jérôme Gaillardet [b,*], JiuBin Chen [a], Ting Zhang [a], Hongming Cai [a], Wei Yuan [a], Zhongwei Wang [d]

[a] *School of Earth System Science (SESS), Institute of Surface-Earth System Science (ISESS), Tianjin University, 92 Weijin Road, 300072 Tianjin, China*

[b] *Université de Paris, Institut de Physique du Globe de Paris, CNRS, F-75005 Paris, France*

[c] *Laboratoire d'Hydrologie et de Géochimie de Strasbourg (LHYGES), CNRS, Université de Strasbourg, 1 rue Blessig, 67084 Strasbourg, France*

[d] *Institute of Geochemistry, Chinese Academy of Sciences (CAS), 99 West Lincheng Road, 550081 Guiyang, China*

Received 6 April 2021; accepted in revised form 12 August 2021; Available online 19 August 2021

Abstract

Lithium (Li) isotopes signatures in sedimentary archives are promising proxies to reconstruct paleo-weathering rates and paleo-seawater composition. Nonetheless, the interpretation of the seawater Li isotope composition evolution over the Cenozoic is still debated. In this aim, the study of large rivers can provide constraints for continental weathering flux to the ocean. However, in the recent past, human activities like flow regulation via reservoir construction, have significantly modified the hydrodynamic of riverine systems, impacting the transfer of matter from the continent to the ocean. Hence, these effects need to be considered and investigated when unravelling the signature of natural processes from river borne materials.

We report Li concentrations and Li isotope compositions (δ^7Li) for the dissolved and sediment loads of subtropical river waters from the Xijiang basin, the largest tributary of the Pearl River (also known as the Zhujiang), Southern China. These rivers display low dissolved Li concentrations. Although they are potentially impacted by carbonate dissolution in the upstream karst terrains, the Li budget of these rivers is dominated by silicate weathering. The dissolved Li isotope compositions of rivers vary over a range from +16‰ to +27‰. These values are high compared to the estimated composition of the bedrock (~0‰), and are explained by the preferential incorporation of the light ^{6}Li in solid weathering products formed during the incongruent dissolution of silicate rocks. We show that the variations of the dissolved δ^7Li values across the basin reflect changes in silicate weathering intensity which controls the formation of secondary phases. The high δ^7Li values in the headwaters reflect greater degree of secondary phase formations associated with the higher erosion rates in the mountainous part of the basin, whereas the lower δ^7Li values in the lowlands characterized by low soil erosion rates and more abundant rainfall reflect a more intensive weathering. This interpretation is supported by the positive relationship between soil erosion rates and the Li dissolved fluxes. The isotope compositions of the suspended particulate material (SPM) transported by rivers in the Xijiang Basin (from −3.8‰ to −0.7‰) are systematically lower than the composition of the bedrock. We observe that the δ^7Li of most SPM samples collected during the wet season are lower than those of samples collected during the dry season. We interpret this seasonality as a consequence of seasonal changes in the sediment properties due to water regulation. In spite of the influence induced by river managements on the river sediments, our data also highlight that the imprint of weathering

* Corresponding authors.
E-mail addresses: benjam@tju.edu.cn, b.chetelat@yahoo.com (B. Chetelat), gaillard@ipgp.jussieu.fr (J. Gaillardet).

https://doi.org/10.1016/j.gca.2021.08.015
0016-7037/© 2021 Elsevier Ltd. All rights reserved.

and erosion processes is still preserved in the sedimentary load of the Xijiang as suggested by the relationship between the SPM δ^7Li values and the weathering intensity defined as the ratio between the chemical weathering rates and the total denudation rates. Altogether, our study confirms the robustness of Li isotopes as a proxy of weathering and erosion processes, even in this heavily-managed river system.
© 2021 Elsevier Ltd. All rights reserved.

Keywords: Lithium isotopes; Chemical weathering; Pearl River; Xijiang; Weathering intensity; River management

1. INTRODUCTION

The interplay between tectonic and sedimentary processes shapes landscapes and ensures the transfer of matter between the surface and the deep Earth, and plays a crucial role in the long-term evolution of climate via the sequestration of carbon in carbonate rocks (Walker et al., 1981; Berner et al., 1983; Hilton and West, 2020). During the chemical weathering of silicates, primary minerals are partially dissolved, releasing soluble elements into solution and leading to the formation of residual secondary phases such as clay minerals and aluminum/iron oxides. Solutes are rapidly transported to the oceans via runoff while residual solid phases accumulate to form soils, the erosion of which leads to sediment fluxes that are delivered to sedimentary basins by rivers. Because large rivers drain significant portions of the Earth's surface, the study of their dissolved and sediment loads provides spatially-integrated information on chemical and physical weathering processes at a scale that is relevant for global geochemical cycles and climate (Gaillardet et al., 1999a, 1999b).

Among the different isotopic tools developed in the recent years, lithium (Li) isotopes appear to be a potentially powerful proxy of silicate weathering (Huh et al., 1998; Rudnick et al., 2004; Kisakurek et al., 2005; Vigier et al., 2009; Lemarchand et al., 2010; Millot et al., 2010a; Teng et al., 2010; Wimpenny et al., 2010; Clergue et al., 2015; Liu et al, 2015; Henchiri et al., 2016; Weynell et al., 2017; Murphy et al., 2019). Lithium is mainly hosted in silicate rocks, and during chemical weathering Li isotopes (^{6}Li and ^{7}Li) are strongly fractionated, with ^{6}Li being retained in the secondary phases, thereby leaving the solution enriched in the heavy isotope. In addition, Li is not a nutrient and its isotopes are not fractionated during vegetation uptake hence, they are "unsensitive" to cycling by vegetation (Lemarchand et al., 2010; Clergue et al., 2015). For instance, the fractionation of Li isotopes during water/rock interactions has been used as a tracer to study weathering processes in soils (Rudnick et al., 2004; Teng et al., 2010; Ryu et al., 2014) and also to quantify the mass of Continental Crust lost by chemical weathering through geological time scale (Liu and Rudnick, 2011). In this regard, the Li isotope composition of rivers allows for estimating the catchment-scale silicate weathering processes and is revealed to be a proxy of weathering intensity (Huh et al., 2001, Dellinger et al., 2015, 2017) that is the mass fraction of the source rock lost to solution during chemical weathering. Indeed, the magnitude of the enrichment in heavy Li isotope in the riverine dissolved load (or the light Li isotope in the sediments) relative to the composition of the source rock varies with the weathering intensity (Dellinger et al., 2015, 2017). This opens the possibility for using Li isotopes in sedimentary archives to quantitatively reconstruct paleo-seawater Li isotopic composition and paleo-continental weathering intensity (Hathorne and James, 2006; Misra and Froelich, 2012; Dellinger et al., 2017). However, the interpretation of the seawater Li isotope composition evolution over the Cenozoic (Hathorne and James 2006; Misra and Froelich, 2012; Caves-Rugenstein et al., 2019) is still debated, and this evolution was hypothesized to result mainly from a change of the riverine inputs and/or a shift in outputs from the ocean between low and high temperature sinks of Li (see Penniston-Dorland et al., 2017 for a review). For instance, the increase of the seawater Li isotope composition during the Cenozoic has been interpreted as a consequence of the shift of the Li isotopic composition of the riverine inputs from light isotopic composition 60 Ma ago toward the present-day value of +23‰. Such a shift was interpreted to reflect a progressive transition from congruent weathering characterized by low dissolved Li isotopic composition transported by rivers to the ocean toward more incongruent weathering associated with higher secondary minerals' formations rates resulting in higher riverine Li isotopic composition delivered to the ocean, as the consequences of the increasing the tectonic activities and uplift of mountain belts during the Middle/Late Cenozoic (Misra and Froelich, 2012). Alternatively, it was proposed that an increase of the Li flux delivered by rivers to the ocean associated with a slight decrease of the riverine Li isotope compositions could also reproduce the evolution of the seawater Li isotope composition during the Cenozoic (Vigier and Godderis, 2015). Additionally, a shift in the dominant ocean Li sinks towards increased low-temperature outputs associated to the removal of Li by authigenic secondary minerals formation in detrital sediments relative to high-temperature Li removal during weathering of the ocean crust might have contributed to the Cenozoic evolution of seawater Li isotopes (Li and West, 2014). In this aim, the study of Li isotopes in large rivers along climatic and geomorphic gradients can provide constraints for weathering and erosion processes, the continental fluxes to the ocean, and eventually for the interpretations of the seawater Li isotope composition evolution since Cenozoic and the siliciclastic record of chemical and physical erosion processes. However, in the recent past, human activities such as river management and flow regulation via reservoir constructions have significantly modified the hydrodynamics of riverine systems, impacting the transfer of material from the continent to the ocean (Liu et al., 2019; Yang et al., 2019). Hence, these effects have

to be evaluated and potentially considered when unravelling the signature of natural processes from the material transported by large rivers.

In this study, we focus on the Xijiang river, the largest tributary of the Pearl River (also known as the Zhujiang) which is one of the largest Chinese rivers, characterized by intense weathering (Chen et al., 2019) and as well as by an upsurge in dam construction since the 1980s–1990s (Wu et al., 2012). We report Li concentrations and isotopic compositions for both the dissolved and sediment loads of the Xijiang main stream and tributaries. We show that the variation of the dissolved δ^7Li values across the basin reflect spatial shift in silicate weathering intensity, which we relate to the transition from an "intermediate" weathering regime characterized by high proportion of Li incorporated into secondary minerals to a more supply-limited regime characterized by a lower proportion of Li incorporated into secondary minerals. We also discuss the effects of large river management and regulation on sediment transport dynamics as well as their potential impact on the river geochemical fingerprints of basin scale weathering processes.

2. STUDY AREA, SAMPLING, AND ANALYTICAL METHODS

2.1. Study area

The Pearl River is the second largest river in China in terms of annual discharge (220 km^3/yr). The Pearl River originates from the Yunnan-Guizhou plateau and flows from the northwest to the southeast into the South China Sea, and mainly consists of three sub-basins: the Xijiang, the Beijiang, and the Dongjiang. In this study, we focus on the Xijiang river, which occupies 78% of the Pearl River total basin area, and accounts for 64% of the Pearl River water discharge (Zhang et al., 2007; Wu et al., 2012). The Xijiang main stream is geographically divided into three sections (Fig. 1): the section upstream from its junction with the Liujiang constitutes the Upper Reach, where the mainstem successively takes the names of Nanpanjiang and Hongshuihe. The Middle Reach extends downstream to Wuzhou city, and there the river is named first the Qianjiang and then the Xunjiang. The Lower Reach constitutes the last section where the main stream becomes the Xijiang. The largest tributaries of the Xijiang are the Beipanjiang in the Upper Reach, as well as the Liujiang, the Yujiang, the Guijiang, and the Hejiang in the Middle Reach. Carbonate rocks outcrops, consisting in both limestones and dolomites, cover 45% of the total basin area and are principally abundant in the Upper and Middle reaches where karstic features are well developed. Siliciclastic sedimentary rocks (shales, sandstones, and siltstones) are also widely distributed in the Upper Reach, while Quaternary fluvial sediments are abundant in the fluvial plains of the Middle and Lower reaches. Igneous rocks, dominated by granitoids, are particularly present in the Middle and Lower reaches, whereas basic volcanic rock outcrops are only reported in the Upper Reach (Zhang et al., 2007; Xu and Liu, 2010; Hu et al., 2013; Fig. SI 1). Limestone red soils and lateritic red soils are widely distributed across the basin. Paddy fields are abundant in the headwaters of the Xijiang and in the Pearl River delta plain (Xu and Liu, 2010).

Straddling the Tropic of Cancer, the Xijiang basin experiences a subtropical to tropical monsoon climate, strongly affected by East Asian and South Asian monsoons. The mean annual temperature ranges between 14 ℃ and 22 ℃, and the mean annual precipitation ranges from 1200 to 2200 mm, both decreasing from east to west. Precipitation is unevenly distributed through the year and its intensity is controlled by the monsoon. As a consequence, more than 80% of the annual river runoff occurs between April and September (Zhang et al., 2007). Spatial variation of the annual runoff across the basin (Döll et al., 2003) follows the distribution of the rainfall as illustrated in Fig. SI 2. Runoff varies from around 500 mm in the northwestern part of the basin to more than 1500 mm in the southeastern part. Conversely, modeled soil erosion rates (Borrelli et al., 2017) generally decrease from the mountainous areas located in the western part of the basin to the lower-altitude areas in the eastern part of the basin (Fig. SI 3).

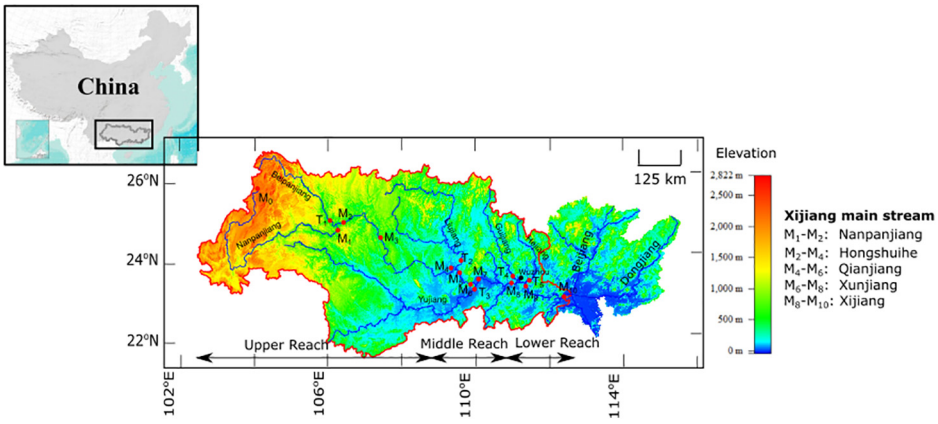

Fig. 1. Map of the Pearl River basin (Linke et al., 2019) with the sampling locations (red dots) (N.B: To avoid, the overlapping of the dots at the confluences because of the scale, sampling points have been moved from their exact locations). The limit of the Xijiang basin is indicated by the red contour. ASTER GDEM elevation data were used to draw the topography of the basin.

During the past decades, river impoundment/damming (Fig. SI 4) and seasonal regulation of water storage have modified water and sediment transport in the Pearl River (Zhang et al., 2007; Zhang et al., 2008). The maximum discharge during the wet season has been shown to decrease, whereas the water discharge during the dry season has been shown to increase, both observations being attributed to water storage regulation in reservoirs (Zhang et al., 2012). In addition, the average annual sediment load of the Pearl River calculated since 2006 is only 30% of that reported for the period 1950–1980 (Wu et al., 2012). Although this decrease of sediment flux in the Pearl River has been observed all year around, its impact in the dry season is less marked because it corresponds to the period when water is released from the reservoirs (Wu et al., 2012).

2.2. Sampling

River samples (dissolved load, suspended load, bed sands, and bank sediments) were collected along the Xijiang main stream and its major tributaries during the wet season in June 2015 and during the dry season in December 2015 (Fig. 1). For each sampling location, 5 to 10 L of river water were collected near to the surface. The dissolved and suspended loads were isolated within 24 hours after collection by filtration through 0.22-μm porosity cellulose acetate filter membranes (142 mm diameter). Water samples for cations, trace elements, and Li isotope analyses were acidified to pH < 2 using ultra-pure 16 N HNO_3.

2.3. Analytical methods

2.3.1. Dissolved major and trace element concentrations

Major cations and trace element concentrations were analyzed by ICP-OES (VISTA-MPX) and ICP-MS (Agilent 7500), respectively, at the State Key Laboratory for Environmental Geochemistry (SKLEG), Chinese Academy of Sciences (CAS), Guiyang with a precision better than ± 10%. Major anions were measured by ion chromatography (Dionex ICS-90) at SKLEG with a precision better than ± 10%. Accuracy and precision were checked and estimated based on the replicated analysis of standard solutions (multi-element calibration standards 1, 2A, 3 and 4 from Agilent Technologies, Japan) and samples.

2.3.2. Sediment major and trace element concentrations

Sediment samples were first crushed in an agate mortar to 200 mesh. About 50 mg of each sample were then digested using a 1:3 mixture of distilled HNO_3 and HF, followed by aqua regia and 6 N HCl, until a clear solution was obtained.

Major cations and trace element concentrations were analyzed by ICP-OES (VISTA-MPX) and ICP-MS (Agilent 7500), respectively at SKLEG with a precision better than ± 10%. Lithium concentrations were determined by ICP-MS (Agilent 7900) at the Institute of Surface-Earth System Science (ISESS) Tianjin University using rhodium as an internal standard with a precision better than ± 10%. In order to ensure the accuracy and precision of the Li concentration analysis, two processes have been set (1) for each batch of samples, three samples have been duplicated, including digestion and measurement (2) several standards have been analyzed including basaltic rock standards JB-2 and BHVO-2, as well as several Chinese national standards for stream sediments (GSD-9, GSD-10, GSD-4A, and GSD-7A).

2.3.3. Lithium isotopes

Solution aliquots of digested sediment samples and of water samples containing 25 ng Li were evaporated at 90 °C and then re-dissolved in 0.5 ml 1 N HNO_3 for chemical separation. For water samples, an aqua regia treatment was employed prior to re-dissolution in order to remove organic matter. Chemical separation of Li from the matrix was achieved by a two-step column chromatography procedure (Zhang et al., 2021) based on a cation exchange resin (Biorad AG50W-X12, 200-400 mesh). At each step, the sample was loaded onto a column filled with 1 ml resin and Li was separated from the matrix using 1 N HNO_3 or 0.2 N HNO_3 as eluents. The Li eluate was evaporated and treated with aqua regia for several days to prevent potential matrix effects from dissolved organic matter during MC-ICP-MS analysis (Kuessner et al., 2019). Finally, the solution was evaporated and re-dissolved in 1 ml 0.5 N HNO_3.

Li isotope ratios were measured by MC-ICP-MS (Thermal Scientific, Neptune plus) at the PARI platform at the Institut de Physique du Globe de Paris (IPGP) and at ISESS. A standard-sample bracketing (SSB) method was used to correct for instrumental mass fractionation, and all the isotope values are reported as per mil (‰) deviations relative to the reference material NIST RM 8545, also commonly referred as L-SVEC:

$$\delta\ ^{7}Li = \left(\frac{2 \times [\ ^{7}Li/\ ^{6}Li]_{samp}}{[\ ^{7}Li/\ ^{6}Li]_{std1} + [\ ^{7}Li/\ ^{6}Li]_{std2}} - 1 \right) \times 1000 \qquad (1)$$

where the subscripts *samp*, *std1*, and *std2* refer to the sample, and the standard (L-SVEC) measured before and after the sample measurement, respectively.

Accuracy and reproducibility of measurements were checked through repeated analyses of various types of reference materials. Repeated measurements of IRMM-016 (lithium carbonate), JB-2 (basaltic rock), and NASS-7 (seawater) respectively yielded δ^7Li values of +0.2 ± 0.5‰ (±2σ, n = 54), +4.5 ± 0.5‰ (±2σ, n = 26, three digestions), and +30.7 ± 0.8 (±2σ, n = 26), all of which are in good agreement with published values (Ryu et al., 2014; Clergue et al., 2015; Dellinger et al., 2015). Additionally, duplicates of 13 samples were measured, yielding values different by less than 0.5‰ from the first measurements.

3. RESULTS

The chemical composition of river waters and the origin of major solutes in the Xijiang river have been extensively discussed in previous studies (Xu and Liu, 2007, 2010; Zhang et al., 2007; Jiang et al., 2018). All these studies have concluded on the predominance of carbonate weathering and highlighted the potential contribution of anthropogenic

inputs. Therefore, in this work, we will not discuss the chemical composition of river waters in general, and limit the corresponding discussion on major solutes (Table SI 1) to the aspects that are relevant to constrain the sources of dissolved Li.

3.1. Dissolved Li concentration and isotope composition

The Li concentrations in river waters vary between 0.068 μmol/L and 0.189 μmol/L and show no clear difference between the dry and the wet seasons, with respective average of 0.114 μmol/L and 0.110 μmol/L (Table SI 2). These values are much lower than the worldwide average Li concentration of river water (0.215 μmol/L- 0.265 μmol/L) (Huh et al., 1998; Misra and Froelich, 2012; Froelich and Misra, 2014), as well as than almost all other large river systems that have been studied so far. For instance, the Mackenzie, the Amazon, the Changjiang (Yangtze River), the Ganges, and the Huanghe (Yellow River) display a mean dissolved Li concentration of 0.488 μmol/L, 0.320 μmol/L, 1.259 μmol/L, 0.785 μmol/L, and 2.800 μmol/L, respectively (Millot et al., 2010a; Dellinger et al., 2015; Wang et al., 2015; Pogge von Strandmann et al., 2017; Gou et al., 2019). The Xijiang main stream and tributaries draining mountainous areas in the Upper Reach are generally characterized by higher dissolved Li concentration (0.138 μmol/L-0.189 μmol/L), compared with the Middle and Lower reaches (0.068 μmol/L-0.117 μmol/L).

The dissolved δ^7Li values (thereafter referred to as δ^7Li_{diss}) of the Xijiang mainstream range between +18.1‰ and +25.2‰, and overall decrease downstream (Table SI 2). The δ^7Li_{diss} values of the tributaries show a slightly larger range of variation from +15.1‰ to +27.2‰ (Table SI 2). This range is smaller than those observed in other world large river basins, such as the Mackenzie (+9.3‰~+29.0‰; Millot et al., 2010a), the Amazon (+1.2‰~+32.9‰; Dellinger et al., 2015), the Lena River (+7.1‰~+41.9‰; Murphy et al., 2019), and the Changjiang (+7.6‰~+42.9‰; Wang et al., 2015), but is close to that of the Ganges (+10.7‰~+24.8‰; Pogge von Strandmann et al., 2017) and that of the Congo River (+14.7‰~+22.1‰; Henchiri et al., 2016). The δ^7Li_{diss} values display significant seasonal variations with river water during the wet season which shows systematically higher values than the dry season (Fig. 2a).

3.2. Li concentration and isotope composition in suspended sediments

The Li concentrations of river SPM range between 44 μg/g and 66 μg/g over the two sampling seasons (Table SI 2), with a mean value of 54 μg/g. This is significantly higher than the average Li concentration of the Upper Continental Crust (UCC, 35 ± 11 μg/g; Teng et al., 2004). During the wet season, the SPM Li concentration gradually increases along the mainstream whereas during the dry season, no clear longitudinal variation is observed (Table SI 2). The δ^7Li values of the suspended sediments (hereafter δ^7Li_{SPM}) are much lower than the δ^7Li_{diss} values and vary within a range between −3.8‰ and −0.7‰ (mean value: −2.0‰; Table SI 2). These values are slightly lighter than the estimated Li isotopic composition of the UCC (+0.6 ± 0.6‰ or 0 ± 2‰; Teng et al., 2004; Sauzeat et al., 2015) and those measured in SPM of some other world large rivers such as the Huanghe (+0.6‰~+3.5‰, mean value of +1.8‰; Gou et al., 2019), the Mackenzie (−2.7‰~+3.2‰, mean value of −0.6‰; Millot et al., 2010a; Dellinger et al., 2014), or the Ganges-Brahmaputra (−2.6~+2.9‰, mean value of −0.5‰; Dellinger et al., 2014; Pogge von Strandmann et al., 2017), but are within the range of the values reported for the Changjiang (−4.7‰~+0.7‰, mean value of −1.5‰; Wang et al., 2015) and the Amazon (−3.6‰~+1.7‰, mean value of −2.2‰; Dellinger et al., 2014). One of the most striking features of our δ^7Li_{SPM} dataset is that dry season values are systematically higher than those observed during the wet season (Fig. 2b) in the Middle and Lower Reaches.

3.3. Li concentration and isotope composition in bed and bank sediments

Compared to suspended sediments, river bed and bank sediments (hereafter called indifferently "bed sediments") are characterized by lower Li concentration and higher Li isotope composition, in agreement with what is reported for other riverine systems (Kisakurek et al., 2005; Dellinger et al., 2014). The Li concentration in bed sediment samples from the Xijiang basin ranges from 15 μg/g to 47 μg/g, with an average of 30 μg/g (Table SI 3), similar to the average Li concentration (35 ± 11 μg/g) of the UCC (Teng et al., 2004). The bed and bank sediment δ^7Li values range from −1.3‰ to +6.4‰ (Table SI 3), with most of the data clustering in a relatively narrow range, between −1.3‰ and +3.4‰ (median of +0.9‰), similar to the average value of 0 ± 2‰ estimated for the UCC (Teng et al., 2004). This range is similar to that observed in other world large rivers like the Mackenzie (−1.5‰~+4.1‰) (Millot et al., 2010; Dellinger et al., 2014) and the Amazon (−1.4‰~+3.9‰) (Dellinger et al., 2014).

4. DISCUSSION

In this section, we first discuss the sources of river dissolved and particulate Li in the Xijiang basin. Then we provide interpretation for the observed Li isotope composition in both dissolved and particulate loads in terms of basin-scale weathering intensity. Finally, we discuss the potential effects of damming on the river sediment geochemistry.

4.1. Sources of dissolved lithium in river water

Previous studies concluded that dissolved Li in river water is predominantly derived from the weathering of silicate minerals, even in carbonate-dominated catchments,

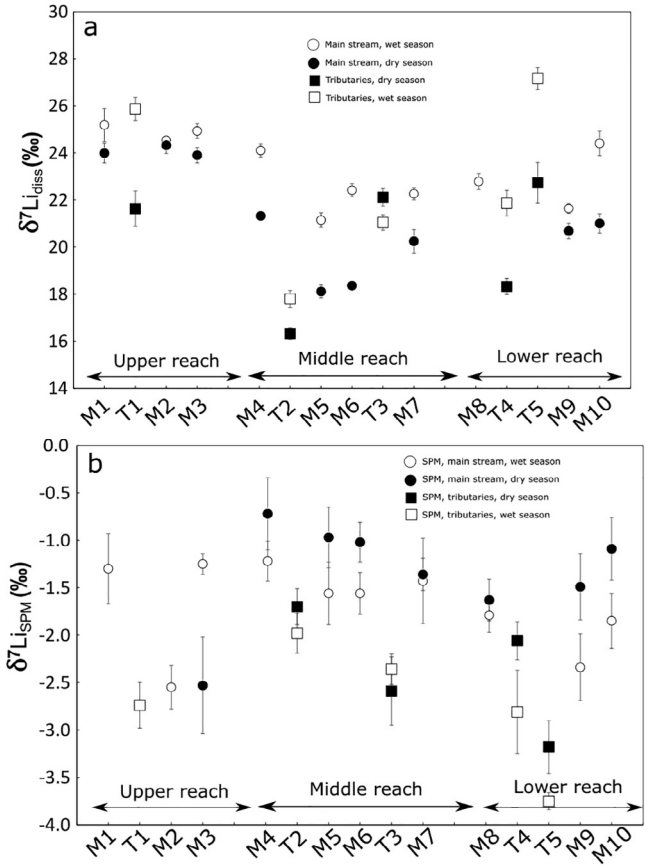

Fig. 2. Spatial and temporal evolution of the Li isotope composition of the dissolved load (a) and suspended particulate matter (SPM) (b) in the Xijiang main stream (circles) and its tributaries (squares).

because of the low Li content in carbonates compared to that in silicate rocks (Huh et al., 1998; Kısakurek et al., 2005; Millot et al., 2010a; Pogge von Strandmann et al., 2017). In the relatively Li-poor river waters of the Xijiang basin, the potential contribution of non-silicate-weathering-derived sources including atmospheric deposition, carbonate and evaporite weathering, and anthropogenic inputs has to be evaluated.

4.1.1. Atmospheric deposition

The atmospheric inputs to river dissolved solutes can be critical for dilute waters. In the atmospheric deposition, Li mainly originates from terrigenous dusts and marine aerosols (Millot et al., 2010a, 2010b). To estimate the contribution of atmospheric inputs to the Xijiang dissolved Li, we adopted the approach of Dellinger et al. (2015). Assuming that the terrigenous dusts have a "local" origin and thus that the terrigenous dusts are an internal source of Li, we consider only sea-salt aerosols as an external source of Li to the catchment. The correction of such "cyclic" (*i.e.*, seawater-derived) salt is usually based on the assumption that chlorine (Cl) in river water is solely of marine origin. For any element of interest X, the concentration derived from cyclic salt inputs, $[X]_{cyclic}$, can be expressed as:

$$[X]_{cyclic} = [Cl]_{river} \times \left(\frac{X}{Cl}\right)_{seawater} \quad (2)$$

In the case where marine aerosols are not the only source of dissolved Cl, a maximum cyclic Cl concentration, $[Cl]_{cyclic}$, has to be estimated first in order to evaluate the upper limit of the cyclic contribution to element X. Then, equation (2) becomes:

$$[X]_{cyclic} = [Cl]_{cyclic} \times \left(\frac{X}{Cl}\right)_{seawater} \quad (3)$$

We use a $[Cl]_{cyclic}$ of 10 μmol/L^{-1} based on previous estimations for the Pearl River and Xijiang basins (Zhang et al., 2007; Jiang et al. 2018). By taking a value of 1.5×10^{-5} for the modern seawater Li/Cl molar ratio, we estimated that the maximum contribution of cyclic salts to the dissolved Li budget in the Xijiang is $< 0.2\%$ averaged over all samples collected during the two seasons. Hence, no attempt is made thereafter to correct for the atmospheric deposition to the Xijiang dissolved Li budget.

The same type of calculation can be performed for other elements, yielding a cyclic contribution that does not exceed 1% for any major cation except for sodium (Na). In the case of Na, the cyclic contribution is between 5% and 10% for most of the samples and can be up to 15%-20% for a small number of samples.

4.1.2. Evaporite dissolution and anthropogenic inputs

After correcting for the contribution of cyclic Cl, river water samples present residual Cl in excess to this contribution (referred to as $[Cl]_{excess}$). This excess highlights the contribution of other sources to the riverine budget of dissolved Cl and potentially of other elements. Dissolution of Cl-bearing evaporite rocks (mostly halite) and anthropogenic inputs are the main candidates to explain the Cl excess. After correction for cyclic contribution, about half of the samples display Cl/Na molar ratios greater than 1, suggesting that halite dissolution is not the main source of the chlorine excess. In addition, the relatively high concentrations of nitrate in the Xijiang also suggest an anthropogenic contribution to the riverine solute budgets, probably associated with agricultural practices within the basin. Previous studies noted the absence of evaporite strata in the Middle and Lower Reaches of the Xijiang basin (Jiang et al., 2018), and stress the impact of anthropogenic activities on the dissolved Cl and NO_3 in the rivers of the Xijiang basin (Zhang et al., 2007; Xu and Liu, 2010; Jiang et al., 2018). First, we assessed the impact of halite dissolution and anthropogenic inputs on solute fluxes by considering that evaporite are absent in the Middle and Lower Reaches (Jiang et al., 2018) and that evaporite dissolution accounts for the entirety of the Cl excess in the Upper Reach (samples M_1, M_2, and T_1). Thus, with the exception of the Beipanjiang (T_1), the Cl excess for all other tributaries is not derived from the dissolution of evaporite but from anthropogenic inputs. For the samples located in the Upper Reach (ie. M_1, M_2 and T_1), the NO_3/Cl molar ratios greater than 1 (1.1–1.6) would suggest that the Cl excess is not entirely derived from evaporite dissolution and would indicate an anthropogenic contribution probably from agricultural activities. Hence, contribution from evaporite to the Cl budget is maximized when assuming that all the excess of Cl in the Upper Reach comes from the evaporite dissolution. In the absence of other sources of Cl, the evolution along the main channel of the Cl excess associated with evaporite dissolution should obey a "dilution" and at each sampling site, the theoretical concentration of Cl derived from the dissolution of evaporite can be calculated using the water discharges. As the data from hydrological stations are limited and do not cover all the sampling sites, we used modeled, long-term annual average water discharge of the Xijiang River and tributaries (Döll et al., 2003). The modeled annual average water discharge is well proportional to the discharge for December 2015 and June 2015 measured at the closest gauging stations (Pearl River Water Resources Commission) (Fig. SI 5) to the sampling sites, although the two sets of estimates differ in absolute value.

$$[Cl]^{M_i}_{excess,evaporite} = [Cl]^{M_2}_{excess,evaporite} \times \left(\frac{Q_{M_2}}{Q_{M_i}}\right) \quad (4)$$

where $[Cl]^{M_i}_{excess,evaporite}$ and $[Cl]^{M_2}_{excess,evaporite}$ are the concentrations of the excess of Cl derived from evaporite dissolution at any sampling point, M_i, along the main channel and at the sampling point M_2, respectively. Q_{M_2} and Q_{M_i} are the water discharges at the sampling points M_2 and M_i, respectively. Contribution from halite dissolution to the river dissolved Na and Li budget can be then estimated by assuming a Na/Cl molar ratio of 1 and a Li/Cl molar ratio of 3×10^{-5} (Millot et al., 2010; Dellinger et al., 2015). In that case the contribution from evaporite dissolution to the dissolved Na along the main stream vary from 8% to nearly 30% during the wet season and from 15% to 70% during the dry season. For the dissolved Li, contribution from evaporite dissolution is less than 2% in both seasons. Assuming a seawater-like δ^7Li of +31‰ for halite, the correction on the Li isotopic composition would be less than 0.1‰ during the wet season and less than 0.2‰ during the dry season. Hence, the effect of evaporite dissolution on the dissolved Li budget and Li isotopic compositions are negligible.

Once corrected from atmospheric inputs and evaporite dissolution, with the exception of one sample (M_3, dry season), samples collected along the main stream in the Middle and Lower Reaches, still present an excess of dissolved Cl and the general evolution of this excess of Cl is an increase from upstream to downstream. When this excess is compared to the dissolved Na corrected from cyclic and evaporites inputs, we observe a general increase from upstream to downstream of the Cl/Na molar ratio (Fig. SI 6).

We interpret the general increase of the Cl/Na ratio as a consequence of anthropogenic inputs characterized by relatively high Cl/Na ratio that we attribute to farming activities as usually industrial and domestic waste waters display low Cl/Na ratios (<1) (Roy et al., 1999). Thus, we use Cl concentrations corrected from atmospheric and evaporite inputs, $[Cl]^{anthro.}_{excess}$, to correct Li and Na concentrations from agricultural inputs. Proportions of lithium derived from anthropogenic inputs are estimated based on the Li/Cl ratio measured in a paddy field water sample collected in this study (1.0×10^{-5}; Tables SI 1 and SI 2) according to:

$$[Li]_{anthro.} = [Cl]^{anthro.}_{excess} \times \left(\frac{Li}{Cl}\right)_{anthro.} \quad (5)$$

where *anthro.* stands for "anthropogenic". The Li contribution from anthropogenic input is on average 1% (from 0% to 2%). Assuming a Li isotopic composition of +24‰ for the anthropogenic inputs associated to farming activities (Gou et al., 2019), the correction on the Li isotopic composition is less than 0.1‰ for all the samples and hence, and is considered as negligible. With the same approach, we estimated the contribution of anthropogenic activities to the riverine Na budget:

$$[Na]_{anthro.} = [Cl]^{anthro.}_{excess} \times \left(\frac{Na}{Cl}\right)_{anthro.} \quad (6)$$

with $(Na/Cl)_{anthro.} = 0.1$ based on the Na/Cl measured in the same paddy field water sample. In that case, Na contribution from anthropogenic inputs vary from 0% to 11% and accounts for 6% on average of the dissolved Na. In a second calculation, we maximized the contribution from anthropogenic inputs associated to agriculture practices, by assuming that all the Cl excess in the rivers from the Xijiang basin (including in the Upper Reach) comes from agriculture. By using Eqs. (5) and (6) (in that case without correction from evaporite), the contribution from agriculture to the dissolved Li budget ranges from less than

0.5% to nearly 2.5%. For the dissolved Na, the contribution in that case varies from 2% to 11%.

Hence, contributions from evaporite and anthropogenic inputs to the Li budget are minor and have no significant effect on the isotopic compositions of the riverine dissolved Li. For the fraction of dissolved Na derived from silicate weathering, $Na_{sil.}$, we used the average of two values calculated either by maximizing the contribution from evaporite dissolution or by maximizing the contribution from anthropogenic inputs. For other major cations, after correction for the cyclic contribution, we assumed that the remaining load was derived from the weathering of carbonate and/or silicate rocks.

4.1.3. Relative contributions from carbonate and silicate rocks weathering

Although the concentration of Li in carbonate rocks (generally ~ 1 ppm or lower; Hathorne and James, 2006; Misra and Froelich, 2012; Andrews et al., 2020) is at least one order of magnitude lower than in most silicate rocks (Tomascak et al., 2016), the widespread distribution of carbonate rocks within the Xijiang basin (especially in the Upper Reach) and the low river dissolved Li concentrations warrant an estimation of the contribution of carbonate rock weathering to the riverine dissolved Li budget in this catchment.

For this calculation, we consider two extreme scenarios. In the first one, the congruent dissolution of carbonates and the incongruent dissolution of silicate minerals constitute two sources of solutes which mix to form the riverine dissolved load. This case would take into account the fastest kinetic dissolution of carbonate rocks and/or corresponds to the mixing of two rivers with one draining exclusively carbonate rocks and the other one draining exclusively silicate rocks. In the second scenario, we consider the case where water percolates through a mixed lithology where dissolved products of carbonate and silicate rocks weathering interact before forming the riverine dissolved load. In this situation, dissolved Li derived from the dissolution of carbonate rocks can eventually be incorporated into secondary minerals derived from the incongruent dissolution of silicate minerals.

In the first scenario, the contribution of carbonate dissolution to the riverine dissolved Li load, $[Li]_{carb.}$, can be calculated according to:

$$[Li]_{carb.} = [Ca]_{carb.} \times \left(\frac{Li}{Ca}\right)_{carb.} \quad (7)$$

where $[Ca]_{carb.}$ is the concentration of dissolved calcium (Ca) derived from the congruent dissolution of carbonates, and $(Li/Ca)_{carb.}$ the molar ratio in carbonate rocks of 1.5×10^{-5} (Kısakűrek et al., 2005; Millot et al., 2010a; Dellinger et al., 2015). After atmospheric correction, we assume that the remaining Ca is exclusively derived from weathering of both silicate and carbonate rocks. Therefore, we can calculate the fraction of Ca derived from the congruent dissolution of carbonates, $[Ca]_{carb}$:

$$[Ca]_{carb.} = [Ca]_{riv.} - [Cl]_{cyclic} \times \left(\frac{Ca}{Cl}\right)_{seawater} - [Na]_{sil.} \times \left(\frac{Ca}{Na}\right)_{sil.} \quad (8)$$

where $[Ca]_{riv.}$ is the dissolved calcium concentration measured in the river water. $[Na]_{sil.}$ is the concentration of Na derived from the weathering of silicate rocks (remaining Na after correction from cyclic, evaporites and anthropogenic inputs, see above), and $(Ca/Na)_{sil.}$ the molar ratio associated with the weathering of silicate rocks. For this calculation, we assumed a $(Ca/Na)_{sil.}$ molar ratio of 0.4 (Zhang et al., 2007; Xu and Liu, 2010). Combining Eqs. (7) and (8), the estimated contribution of pure carbonate weathering to the dissolved Li load in the Xijiang basin varies from 7% to 19% during the wet season and from 8% to 23% during the dry season.

To evaluate the sensitivity of δ^7Li_{diss} to carbonate weathering, we assumed two extreme Li isotopic compositions for the carbonate end-member, +6‰ and +25‰. These two values set the limits of the range of the Cenozoic carbonate isotopic compositions (Misra and Froelich, 2012) and at the Permian-Triassic boundary (Sun et al., 2018). Unsurprisingly, when the δ^7Li value of the carbonate end-member is set at +25‰, relatively close to the riverine Li dissolved isotopic compositions, carbonate dissolution has a limited impact on the river δ^7Li values whereas in the case the carbonate end-member value is set at +6‰, river water river δ^7Li can be lowered by up to 5‰ by carbonate dissolution.

In the second scenario, we assume that Ca and Na are conservative in solution (not re-incorporated into secondary phases) and that Li is released to solution in stoichiometric proportions with Ca and Na from carbonate and silicate rocks, respectively. We can then estimate $[Li]_{init.,carb.}$ (Eq. (9)) and $[Li]_{init.,sil.}$ (Eq. (10)) defined as the "initial" concentrations of dissolved Li (before its incorporation into secondary phases) derived from weathering of carbonate and silicate rocks where $(Li/Na)_{sil.}$ is the Li/Na molar ratio of silicate rocks:

$$[Li]_{init.,carb.} = [Ca]_{carb.} \times \left(\frac{Li}{Ca}\right)_{carb.} \quad (9)$$

$$[Li]_{init.,sil.} = [Na]_{sil.} \times \left(\frac{Li}{Na}\right)_{sil.} \quad (10)$$

Eq. (9) is identical to Eq. (7) but in this scenario, the Li derived from the congruent dissolution of carbonates can be reincorporated into secondary phases resulting from the incongruent dissolution of silicate primary minerals.

The comparison between $[Li]_{init.,carb.}$ and $[Li]_{init.,sil.}$ could provide a first-order estimate of the relative contribution of carbonate and silicate weathering to the dissolved Li budget. However, the estimation of $[Li]_{init.,sil.}$ relies strongly on the knowledge of the composition of the silicate rocks prevailing in the catchment, in particular the relative influence of igneous (mostly granitoid in the Xijiang Nasin) and sedimentary rocks. To account for the fact that the relative contributions of these two rock types to the river dissolved Li budget is unknown, when calculating $[Li]_{init.,sil.}$ using Eq. (10), we vary the fraction of river dissolved $Na_{sil.}$ derived from the weathering of granitoids from 0 to 1 (the remaining be sourced from the weathering of sedimentary rocks). The $(Li/Na)_{sil.}$ values of granitic and sedimentary rocks are 5×10^{-3} and 4×10^{-2}, respectively

(Hu and Gao, 2008; Wang et al., 2013; Dellinger et al., 2014; Xiong et al., 2018). This analysis shows that for most samples the contribution of carbonate weathering to the "initial" dissolved Li budget does not exceed 5% (Fig. SI 7) with the exception of one sample (M_4 collected during the dry season) which shows higher contributions from carbonate dissolution (~11%) in the case where all $Na_{sil.}$ is derived from the weathering of granitoids.

Basic volcanic rocks are also present in the Upper Reach of the Xijiang basin (Fig. SI 1). Therefore, we performed similar calculations as above for the most upstream samples (M_1, M_2, M_3, and T_1) with a fixed, lower $(Li/Na)_{sil.}$ molar ratio in Eq. (10) of 1.5×10^{-3}, representative of volcanic rocks (Dellinger et al., 2014). Results show that for these samples the contribution from carbonate dissolution is small (<5%) depending on the fraction of Na derived from the weathering of sedimentary rocks. In the extreme case where all the Na and Li are derived from the weathering of volcanic rocks, the proportion of Li associated to the weathering of carbonate rocks is on average 10% and can reach 30% for one sample (M_4, collected during the dry season). However, in this case the calculated total initial dissolved Li concentrations ($[Li]_{init.,sil.} + [Li]_{init.,carb.}$) are smaller than the measured dissolved Li concentrations suggesting that Na (and in turn Li) is not entirely derived from the weathering of volcanic rocks but also derived from the weathering of sedimentary rocks. Hence, the contributions from carbonate dissolution are overestimated.

The dissolved Li is Xijiang is likely sourced from processes intermediate between these two scenarios albeit it is challenging to determine exact mechanisms. As shown by the simulations above, carbonate weathering contributes little Li to the river water in Xijiang basin in both scenarios. The overall conclusion of this section is that the source of dissolved Li in the Xijiang basin is thus mainly silicate weathering, in agreement with previous studies on large river basins (Huh et al., 1998; Millot et al., 2010a; Dellinger et al., 2015). As the consequence, the dissolved δ^7Li values mainly reflect isotopic fractionation during the silicate rock-water interaction.

4.2. Sediment provenance and particulate Li sources

We showed above that the dissolved Li in the Xijiang basin is mainly derived from silicate weathering, such that the comparison of Li isotope compositions between source rock and river water might hold clues about silicate weathering processes and intensity (Dellinger et al., 2015). However, silicate rocks display variable Li isotopic compositions (Tomascak et al., 2016; Dellinger et al., 2017; Penniston-Dorland et al., 2017). The Xijiang basin is mostly covered by sedimentary rocks (Fig. SI 1), with igneous rocks accounting for only 16% of outcrops in the catchment (Hartmann and Moosdorf, 2012). In the Xijiang basin, igneous rocks are dominated by granitoids, especially well represented in the Middle and Lower Reaches, whereas volcanic rocks are mainly present in the Upper Reach (Fig. SI 1).

Elemental ratios between insoluble element concentrations in river sediments can be used as fingerprints of the source rocks. In particular, chromium (Cr), vanadium (V), and aluminum (Al) can be considered as immobile during chemical weathering, while their abundances show stark contrat between different type of silicate rocks, such that their elemental ratios have been applied to constrain the nature of the source rocks (Dellinger et al., 2017). The ratios measured in suspended sediments and bedload samples are shown in Fig. 3a. For comparison, we add the range reported for regional siliciclastic sedimentary rocks (Wang et al., 2012; Yang et al., 2012; Wang et al., 2013; Xiong et al., 2018) and Chinese shales (Hu and Gao, 2008) as well as for regional granitoids (Jiao et al., 2015) and basic volcanic rocks (Qi and Zhou, 2008). Bed and suspended river sediments of the Xijiang Basin fall into the Cr/Al-V/Al field defined by the sedimentary rocks. The enrichment in Cr and V observed for some bed sediment and SPM samples could be suggestive of a contribution of basic volcanic rocks. Given the small contribution of basic volcanic outcrop to the Xijiang drainage area (Fig. SI 1), this would imply that the erosion of these rocks contributes disproportionally to the river sediment load. This inference is supported by the fastest soil erosion rates modeled for the Xijiang Upper Reach (Fig. SI 3). Alternatively, if Cr and V are to some extent associated with heavy minerals, mineral sorting alone could explain the larger Cr/Al and V/Al mass ratios observed for some bed sediment samples (Chen et al., 2014). Indeed, the positive relationship between the δ^7Li values and the Cr/Al mass ratio of bed sediments (Fig. SI 8) could be driven by mineral sorting, in which case it would reflect the constitutive mineralogical mixture of sedimentary rocks between detrital clay minerals, enriched in the light Li isotope and detrital primary minerals, enriched in the heavy Li isotope.

The predominance of sedimentary rocks as the source of the river sediments is also supported by the Na/Al and Li/Al mass ratios (Al is assumed to be immobile during weathering) as well as the δ^7Li values measured in the bed sediments. Coarse sediments contain mainly rock fragments (Dellinger et al., 2014), and one approach to constrain at the catchment scale the relative contributions of different rock types would be to assume that the composition of coarse river sediments is representative of the average composition of the rocks drained by the rivers. In the Xijiang, bed sediments are depleted in Na relative to Li compared with igneous rocks and fall into the compositional range defined by regional sedimentary rocks (Fig. 3b), which can be, at a first order, considered as a mixture between fine grain sedimentary rocks (shales) and fragments of igneous rocks type depleted in Na. Regarding the Li isotope composition of the bed sediment samples in the Xijiang basin, they are relatively variable and display a median value of 0.9‰, in the range of values estimated for shales (−2.5‰ - +1.5‰) and lower than the average of igneous rocks at ~ 4‰ (Dellinger et al., 2014). Plotted as a function of the Li/Al mass ratio (Fig. 4), the Li isotopic compositions of most of the bed sediments can be interpreted as well as a mixing between "shale" and "igneous" end-members. We would expect both SPM isotopic compositions and Li/Al ratio to be lower than that of the parent rock because ^7Li is preferentially lost during chemical weathering (or ^6Li is

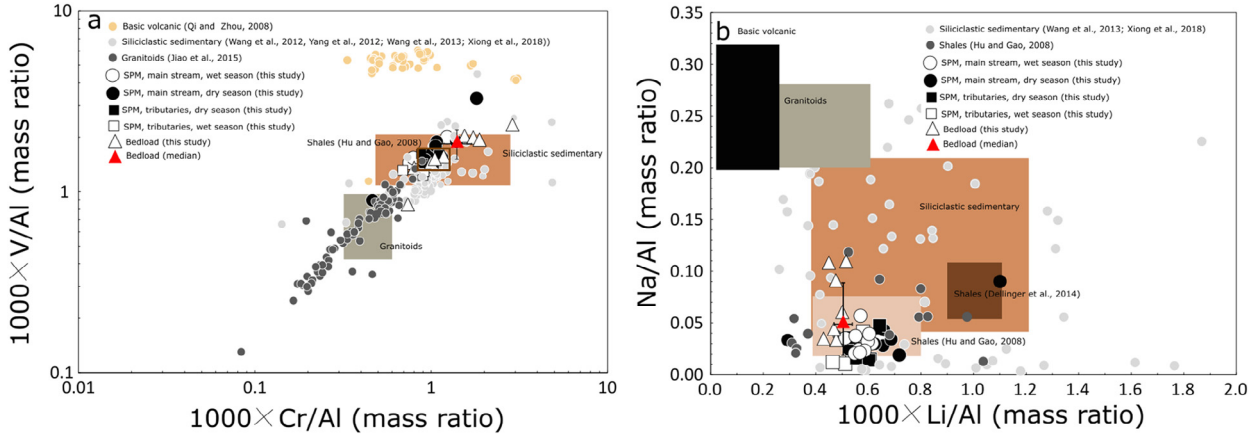

Fig. 3. Elemental ratios, V/Al *vs.* Cr/Al (a) and Na/Al *vs.* Li/Al (b) of the suspended particulate matter (SPM) and bed sediment samples of the Xijiang and its tributaries. Composition of regional rocks and of various relevant rock types are given for comparison. The ranges of variation of the Li/Al ratio for basic volcanic rocks and granitoids are from Dellinger et al. (2014).

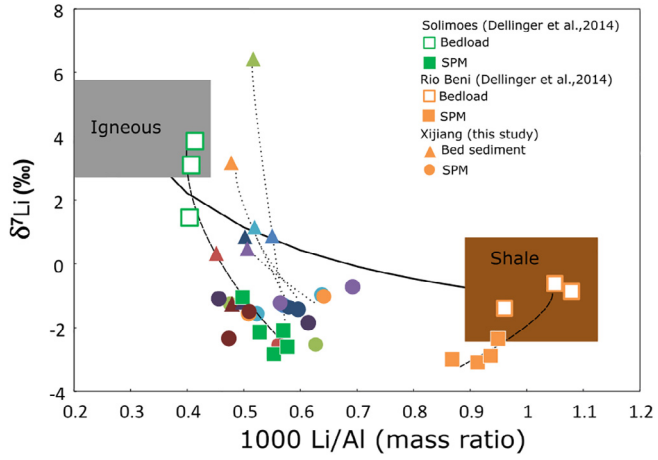

Fig. 4. δ^7Li values *vs.* the Li/Al ratio measured in bed sediments (triangles) and SPM (full circles) collected along the Xijiang main stream. Different colors correspond to different sampling sites where both SPM and bed sediments have been collected. The shale and igneous end-members are from Dellinger et al. (2014). The full black curve is a mixing hyperbola between these two end-members. For comparison, we added the Li isotope compositions measured in the bedload and SPM from the Solimoes, draining both sedimentary and igneous rocks, and the Rio Beni, draining exclusively shale lithology. The dashed and dotted lines indicate the evolution of the δ^7Li values and the Li/Al ratios from coarse (Bedload/Bed sediments) to fine sediments (SPM).

preferentially retained in secondary phases) and because Li is "mobile" whereas Al is supposed to be "immobile". We observe that the SPM are enriched in ^{6}Li compared with the bed sediment as expected, but that the majority of the SPM are characterized by higher Li/Al ratios. This suggests that the "fine" fraction, fragments of unweathered fine sedimentary rocks (shales) characterized by high Li/Al ratio, transports also (and not only products of chemical weathering). Also, this shows the coarse fraction transports relatively more unweathered igneous rocks than unweathered sedimentary rocks. Hence, the Li isotopic composition of bed sediments would represent an upper bound for the Li isotope composition of the bedrock. Such sorting effects and the enrichment of coarse sediments in an "igneous" component have been reported by Dellinger et al. (2014) for most of the world large rivers they studied (Fig. 4). The only exceptional case was when the river drains exclusively shales (Fig. 4).

In regard of the uncertainties on sediment provenance and chemical composition of the source in the Xijiang Basin, we used as a first bound the median composition across the three bed sediment samples with the highest Na/Al ratio in Fig. 3b (this bound reflects a scenario where the contribution of igneous rocks is maximized) for the Li/Na ratio of the bedrock. The other bound is given by the median composition measured across the entirety of the bed sediment sample set. These assumptions result in particular in a mean silicate rock source Li/Na mass ratio of 0.007 ± 0.002. For the isotopic composition of the source rocks, we took as upper bound the median of the δ^7Li

values measured in the bed sediments (+0.9 ‰) and as lower bound, the lowest value measured in the set of bed sediments (−1.3‰) resulting in a mean δ^7Li value of −0.2 ± 1.1‰.

4.3. Variation of dissolved Li isotope composition along the Xijiang mainstream

Downstream variations of river dissolved Li fluxes (Fig. SI 9) and isotopic compositions (Fig. 2a), suggest catchment-scale shifts in Li sources and/or surface processes affecting Li. In this section we discuss the observed evolution of the δ^7Li_{diss} values for the Xijiang mainstream. To this aim, we compare discharge, river solute (including Li) concentrations, and Li isotope composition between pairs of successive samples taken along the Xijiang mainstream. We distinguish three case studies: first, three sampling locations situated at confluences where the Xijiang mainstream has been sampled immediately upstream and downstream from the confluence (as well as the tributary); second, a section of the Xijiang Upper Reach where karstic landforms are prominent, providing an ideal case to highlight a potential effect of carbonate weathering on the river dissolved Li budget; third, a series of river sections in the Middle to Lower reaches where the outcrop of silicate rocks dominates.

4.3.1. Lithium mass balance at confluences in Xijiang basin

Mass balance of solute mixing at river confluences constitutes an opportunity to test the contribution of unaccounted, for example local solute sources to the river system, the validity of the conservative behavior of elements during mixing of water masses (Chen et al., 2008; Guinoiseau et al., 2016, 2018), and the extent of mixing between the water masses downstream from the confluence (Bouchez et al., 2010).

Here we use a set of mass balance relationships describing the evolution of the Li flux and Li isotope ratios at confluences under the assumption that Li behaves conservatively during water mixing:

$$[Li]_{M_{j+1}} = \frac{Q_{M_j} \times [Li]_{M_j} + Q_{T_i} \times [Li]_{T_i}}{Q_{M_j} + Q_{T_i}} \quad (11)$$

$$\delta^7 Li_{M_{j+1}} = \frac{Q_{M_j} \times [Li]_{M_j} \times \delta^7 Li_{M_j} + Q_{T_i} \times [Li]_{T_i} \times \delta^7 Li_{T_i}}{Q_{M_j} \times [Li]_{M_j} + Q_{T_i} \times [Li]_{T_i}} \quad (12)$$

where Q, [Li], and δ^7Li refer to the water discharge, dissolved Li concentration, and dissolved Li isotope composition, and the subscripts "M''_{j+1} and "M_j" designate two adjacent sampling sites along the mainstream, whereas "T_i" designates the tributary located between two adjacent mainstream sampling sites. Here we perform these calculations at the junctions between the mainstream and the three largest tributaries, namely the Beipanjiang (T_1), Liujiang (T_2) and Yujiang (T_3), for which we have close (5 to 15 km apart) adjacent sampling points upstream and downstream of the confluence. For these calculations, we use the modeled water discharge (*cf.* Section 4.1.2). For the three confluences under consideration the estimated values for the dissolved Li concentrations and Li isotope composition after mixing (Eqs. (11) and (12)) are in good agreement with the measured values (Fig. SI 10). This result suggests that in the Xijiang, Li behaves conservatively during water mixing and that no major source of Li is omitted. In addition, this analysis shows that in the Xijiang main stream water masses from tributaries are well mixed over relatively short distances of less than 15 km.

4.3.2. Impact of carbonate dissolution in karstic landforms on the river dissolved Li budget in the Upper Reach of the Xijiang basin

We show above that the contribution of carbonate mineral dissolution to the dissolved Li budget in the Xijiang basin is small. However, limestone formations generally host a significant portion of silicate material (for example present as marl layers, or as disseminated clays within the carbonate layers), meaning that limestones could act as a source of Li to rivers. Here we focus on the Xijiang section between the sampling points M_2 and M_4 (Fig. 1), known to be exempt of large tributaries although the water discharge increases by a factor two. In this region the landscape is dominated by karst features and numerous underground rivers flow (Ma et al., 2002). The influence of carbonate weathering to the river water geochemistry is for instance shown by the increase of the Ca/Na ratio (Fig. SI 11).

To assess dissolved budgets, we compared the elemental inflows and outflows for this section. During the wet season, the dissolved Ca flux increases downstream by a factor of two over this section, whereas the river dissolved Li flux increases by only 20% (using again modeled water discharges *cf.* §4.1.2 and §4.2.1). Assuming that the entirety of the Ca downstream increase is due to carbonate dissolution, and that Li/Ca molar ratio in carbonate is 1.5×10^{-5}, carbonate dissolution would account for more than 60% of the downstream increase of the Li flux. Using the same approach, we calculate that during the dry season, carbonate rock dissolution accounts for more than the observed downstream increase in the river dissolved Li flux. Intriguingly, this Li increase is accompanied with a significant increase of the dissolved Si and K fluxes but not of the dissolved Na flux. Hence, this increase of the Li flux could be due to the dissolution of silicate minerals which are Si-K-rich and Na-depleted contained in the limestone formations. In addition, the downstream decrease in the dissolved Li isotopic composition (by 0.4‰ in the wet season and by 3‰ in the dry season) suggests that this additional source of Li is relatively light. This observation is again compatible with the dissolution of clay minerals enriched in ^{6}Li. The fact that the major variation of the δ^7Li value occurs during the dry season is consistent with a higher contribution of karst groundwater to the base flow. Hence, in this area, the seasonal variation of karst groundwater contribution could contribute to the observed shift of the dissolved Li isotopic composition between the dry and wet seasons.

4.3.3. Behavior of Li in the Middle and Lower reaches of the Xijiang basin

Water-mineral interactions within floodplains can exert a strong control on the downstream evolution of the

riverine Li isotope composition (Bagard et al., 2015; Dellinger et al., 2015; Ma et al., 2020). These changes are associated with either a net removal of Li or with a net additional flux of Li to the river water. For instance, some high dissolved δ^7Li values measured in the lower reaches of the Amazon Basin are explained by a net removal of dissolved riverine Li during the interaction of Li with sediments stored in floodplains, leading to a downstream decrease of the Li flux (Dellinger et al., 2015; Maffre et al., 2020). Alternatively, contribution from unsampled tributaries, groundwater, and/or interaction with sediments deposited in the alluvial plain resulting in a potential net input of dissolved Li to the river water could explain such downstream evolution of the river Li isotopic composition. In the context of the Xijiang Basin, this question can be addressed by examining the variation of the dissolved Li flux (Fig. SI 9) and isotopic composition (Fig. 2a) along the main stream in the Middle and Lower reaches (samples M_7 to M_{10}). In this section, the dissolved Li flux shows a general increase (Fig. SI 9), while the dissolved Li isotope composition generally increases, although not in a monotonous way. Importantly, carbonate dissolution plays there a relatively minor role in the Li budget which is dominated by silicate weathering as evidenced by the smaller increase of the flux of calcium relative to the flux of solutes ($Na_{sil.}$, K and Si) derived from silicate weathering.

Mass balance calculations between the sampling points M_7 and M_8 during the wet season show that the additional Li flux is characterized by a δ^7Li value of +25‰ and that the solute fluxes of Si, K and $Na_{sil.}$ all increase. More specifically inputs characterized by an average $Na_{sil.}$ concentration of 385 μM are necessary to explain the observed increase of $Na_{sil.}$ between M_7 and M_8. By comparison, Xu and Liu (2010) reported a dissolved Na concentration of about 270 μM (once corrected with Eq. (6) from anthropogenic inputs) for the Beiliujiang (unsampled in our study), the largest Southern tributary of the Xijiang in this section of the main stream. The authors report a dissolved $^{87}Sr/^{86}Sr$ ratio of 0.720 for this tributary, compatible with a significant contribution of silicate weathering to its solute load. Hence, contribution from unsampled tributaries could partly explain the observed increase in the silicate weathering flux over this section.

By contrast, similar mass balance calculations made during the wet season between sites M_9 and M_{10} show that the dissolved Li and Si fluxes decrease over this section. Interestingly, this decrease in the Li flux (Fig. SI 9) is associated with an increase in the dissolved Li isotope composition (Fig. 2a), which would be consistent with a net removal of Li (and Si) during water–mineral interactions within the floodplain (e.g. Dellinger et al., 2015).

4.4. Factors impacting Li isotope fractionation during continental weathering in the Xijiang basin

We show that across the Xijiang basin the dissolved Li isotope compositions vary from 16‰ to 27‰ and are enriched in the heavy Li isotope relative to river sediments and bedrock. Given that in the Xijiang basin Li is mainly derived from the chemical weathering of silicate rocks, the observed range of dissolved δ^7Li values mainly result from Li isotope fractionation during the incongruent dissolution of silicate minerals and ensuing formation of secondary minerals, in line with previous studies conducted in both small catchments and large river basins (Huh et al; 1998; Kisakurek et al., 2005; Vigier et al., 2009; Lemarchand et al., 2010; Millot et al., 2010a; Wimpenny et al., 2010; Clergue et al., 2015; Dellinger et al., 2015; Liu et al., 2015; Weynell et al., 2017; Murphy et al., 2019). In the next sections we address what set of processes control this range of dissolved Li isotope signatures in the Xijiang basin.

4.4.1. Role of secondary mineral formation

During the incongruent dissolution of silicate rocks, the incorporation of Li in secondary phases and its adsorption onto mineral surface lead to strong Li isotope fractionation in favor of the incorporation/adsorption of the light ^{6}Li (Huh et al., 1998; Pistiner and Henderson, 2003; Vigier et al., 2008; Dellinger et al., 2015; Gou et al., 2019; Hindshaw et al., 2019; Murphy et al., 2019; Li and Liu, 2020; Zhang et al., 2021). Hence, the fraction of Li remaining in solution becomes enriched in the heavy isotope relative to the parent rock and to the secondary phases.

The fraction of Li incorporated/adsorbed into/onto secondary phases can be estimated by comparing the $Li/Na_{sil.}$ measured in the river water to the Li/Na ratio estimated for the silicate source rock (Millot et al., 2010a; Dellinger et al., 2015; Murphy et al., 2019). This calculation implicitly hinges on the premise that elements Li and Na are released congruently during the dissolution of primary minerals and thus, that the difference in mobility between these two elements is only due to the incorporation of Li into secondary phases (with Na not being retained in these secondary phases):

$$f(Li)_{sec} = 1 - \frac{\left(\frac{Li}{Na}\right)_{sil}}{\left(\frac{Li}{Na}\right)_{bedrock}} \quad (13)$$

where $f(Li)_{sec}$ is the fraction of Li incorporated into secondary minerals, $(Li/Na)_{sil.}$ is the ratio of dissolved Li to Na (both derived from silicate weathering) measured in river water, and $(Li/Na)_{bedrock}$ is the ratio in the bedrock. To estimate $f(Li)_{sec}$ we chose a $(Li/Na)_{bedrock}$ of 0.023 mol/mol, as estimated for the composition of source of the sediments (Section 4.1.2).

With the exception of one sample (T_4, dry season) displaying a relatively low fraction of Li incorporated into secondary phases, $f(Li)_{sec}$ values vary over a narrow range across the Xijiang Basin, between 0.93 to 0.97 (Fig. SI 12). Hence, for most locations, a large proportion of the Li initially released into solution by silicate weathering is reincorporated into secondary phases, which in turn explains the high river dissolved δ^7Li values. Both spatial and temporal variations of $f(Li)_{sec}$ follow roughly the same patterns as those displayed by the dissolved Li isotope composition, indicating that Li isotope fractionation associated with the incorporation of Li in secondary phases explains the observed variation in dissolved δ^7Li values.

Controls on the fraction of Li incorporated into secondary phases on the dissolved Li isotopic compositions is further illustrated in Fig. 5 where we report the dissolved

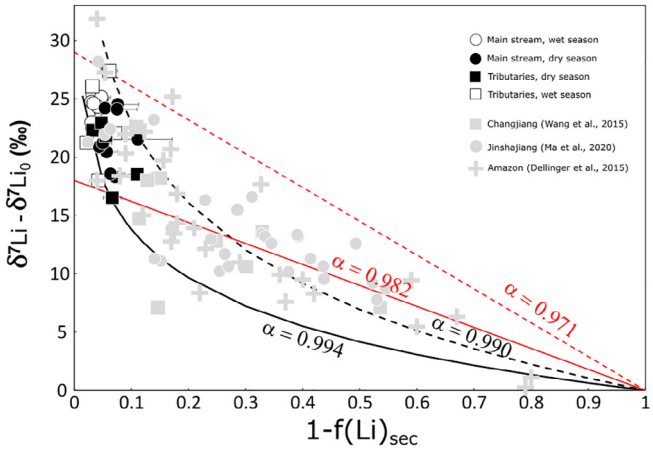

Fig. 5. Dissolved δ^7Li values corrected from the estimated initial composition, δ^7Li_0, of the Xijiang and its tributaries *vs.* the fraction of initial Li remaining in solution after formation of secondary phases (1-f(Li)$_{sec.}$, Eq. (13)). The error bars on the fraction of Li remaining in solution take into account the uncertainties on the Li/Na initial of the bedrock and the uncertainties on the fraction of Na derived from silicate weathering (*cf.* Sections 4.1.2. and 4.2.). By comparison, we also reported data from the literature for the Jinshajiang, the Changjiang and the Amazon (Dellinger et al., 2015; Wang et al., 2015; Ma et al., 2020). The black/red plain and dashed lines are the modeled trends following Rayleigh distillation (black lines) and batch fractionation (red lines) laws, for different values of the Li isotope fractionation factor prevailing during Li incorporation into secondary phases. (For interpretation of the references to colour in this figure legend, the reader is referred to the web version of this article.)

δ^7Li values as a function of the (Li/Na)$_{sil}$ ratio normalized to that of the estimated for the bedrock, *i.e.* the fraction the initial Li remaining in solution after formation of secondary phases, or in other terms 1- f(Li)$_{sec}$.

The evolution of the dissolved Li isotope composition with the fraction of Li remaining in solution can be at a first order explained either by a steady-state, open flow-through fractionation model (Eq. (14)), mathematically equivalent to the so-called "batch" model (Bouchez et al., 2013) or by a Rayleigh distillation model (Eq. (15)) (Dellinger et al., 2015; Murphy et al., 2019).

$$\delta^7 Li_{diss.} = \delta^7 Li_0 - 1000 \times (\alpha - 1) \times f(Li)_{sec.} \quad (14)$$

$$\delta^7 Li_{diss.} = \delta^7 Li_0 - 1000 \times (\alpha - 1) \times ln\left[1 - f(Li)_{sec.}\right] \quad (15)$$

where δ^7Li_0 is the composition of the bedrock (chosen here equal to −0.2‰) and α is the Li isotopic fractionation factor prevailing during Li incorporation into secondary phases.

As observed in previous studies, the range of the fractionation factors to explain the data differs between the two models. Higher values of α (between and 0.990 and 0.994) are required to explain the data with Rayleigh distillation model compared with the range for the open flow-through fractionation model values (between and 0.971 and 0.982). However, these latter values are those typically reported for the incorporation of Li in clay minerals, either from experimental or deduced from field studies (Bagard et al., 2015; Chan et al., 1992, 2002; Dellinger et al., 2015; Hindshaw et al., 2019; Li and Liu, 2020; Ma et al., 2020; Maffre et al., 2020; Murphy et al., 2019; Pistiner and Henderson, 2003; Vigier et al., 2008; Wang et al., 2015; Zhang et al., 1998, 2021). Dependence of the fractionation factor with the type of secondary minerals formed and/or the bonding environment of Li in the secondary minerals ("exchangeable" Li vs. "non-exchangeable" Li or structurally bond Li) have been put forward to explain the range of α values observed in rivers (e.g. Pogge von Strandmann et al., 2017; Murphy et al., 2019; Ma et al., 2020). In this view, lower isotopic fractionation factors are expected to be associated with the incorporation of non-exchangeable Li whereas exchangeable Li is expected to have an isotopic composition closer to that of the solution (Vigier et al., 2008; Wimpenny et al., 2015; Hindshaw et al., 2019). In addition, the high proportion of Li incorporated into secondary minerals associated with the uncertainties on the composition of the bedrock and on the fraction of dissolved Na derived from silicate weathering could also contribute to the range of α values needed to explain the data and hence hamper a clear discrimination between the two models (open flow-through *vs.* Rayleigh distillation) to explain the data. In the following section, we are going to address the factors controlling the formation of secondary minerals and the subsequent incorporation of Li.

4.4.2. Control by weathering regime and the potential role of climate on the Li geochemistry in the Xijiang basin

As Li is ultimately derived from silicate weathering, what might limit the supply of Li to the system is the exposure of minerals to chemical weathering. In supply-limited weathering systems, low physical erosion rates favor the development of thick soils, inhibit the exposure of "fresh" minerals which in turn results in relatively low chemical weathering rates. In this case, a positive relationship between physical erosion rates and Li dissolved fluxes is expected. As illustrated in Fig. 6, in the Xijiang Basin dissolved Li fluxes show a positive relationship with modeled soil physical erosion rates, confirming that the supply of Li by Earth surface denudation is the limiting factor for dissolved Li production there.

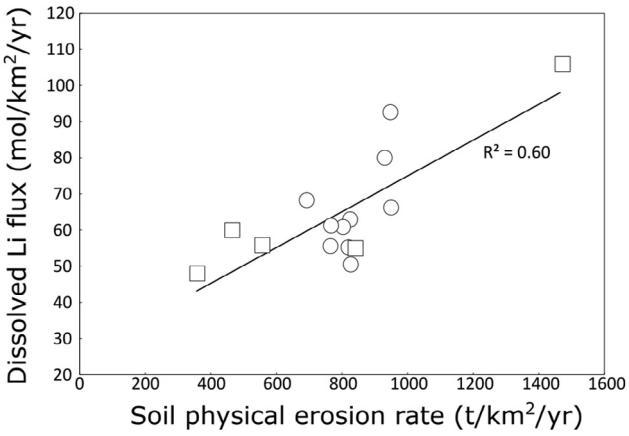

Fig. 6. Relationship between the dissolved Li fluxes calculated for the samples collected during the wet season in the Xijiang main stream (circles) and its tributaries (squares) and the modeled soil physical erosion rates (Borrelli et al., 2017).

In this view, the relatively high physical erosion rate in the basin headwaters enhances silicate weathering rates and in turn would promote the formation of secondary minerals. Therefore, the incorporation of Li in secondary phases explains the high dissolved δ^7Li values observed. On the contrary, in the lowlands, secondary phase formation would be limited, such that the chemical signature of waters would instead be overprinted by the re-dissolution of secondary phases characterized by the release of low Li isotopic composition to waters (Dellinger et al., 2015). This dissolution could be favored by the lower soil erosion rate in the lowlands, which increases the residence time of material in soils resulting in more "intense" weathering. The relationship between the Li isotope compositions and the weathering intensity across the basin is illustrated in Fig. 7 where we use the molar ratio Si/($Na_{sil.}$ + K) as a proxy for the weathering intensity (Stallard and Edmond, 1987). The rationale of this proxy is based on the difference of mobility between the elements during chemical weathering. During silicate weathering, Na and to a lesser degree K are mainly released into solution whereas dissolved Si is partially taken up by secondary minerals. Hence, incongruent dissolution of silicate minerals associated with secondary minerals formation is characterized by low Si/($Na_{sil.}$ + K) molar ratio, whereas more complete dissolution (and dissolution of secondary minerals) is characterized by high Si/($Na_{sil.}$ + K) molar ratio, characteristic of higher weathering intensity. Such correspondence between the dissolved Li isotope composition and weathering intensity has also been observed in other large river basins like the Orinoco basin (Huh et al., 2001). The spatial evolution of the dissolved Li isotopes would thus reflect the transition from an intermediate weathering regime with a higher proportion of Li incorporated into secondary minerals resulting in higher dissolved δ^7Li values to a regime which is supply-limited with a lower proportion of Li incorporated into secondary minerals and hence lower dissolved δ^7Li values. In addition of the physical erosion rate which controls the residence time of the material in soil and thus weathering intensity (Fig. SI 13a), we also note that the downstream increase in silicate weathering intensity could be favored by the increase in rainfall as indicated by the positive

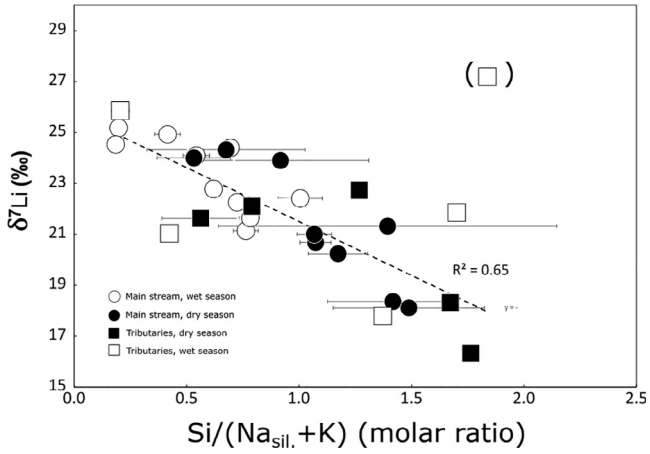

Fig. 7. Dissolved δ^7Li values of the Xijiang and its tributaries *vs.* the Si/(Na_{sil} + K) molar ratio used as a proxy for the silicate weathering intensity. The samples in brackets were excluded from the regression. Uncertainties on the Si/(Na_{sil} + K) take into account the uncertainties on the fraction of Na derived from silicate weathering (*cf.* Section 4.1.2).

relationship between runoff and the Si/($Na_{sil.}$ + K) ratio (Fig. SI 13b). This relationship highlights a possible, climatic control on the weathering intensity and in turn on the dissolved Li isotopic composition of river waters in the Xijiang basin. The observed relationship between the Si/($Na_{sil.}$ + K) ratio and the dissolved Li isotopic composition in the Xijiang basin is opposite to that reported by Ma et al. (2020) for the Yalongjiang (ie. increase of the dissolved δ^7Li values with the Si/($Na_{sil.}$ + K) ratio). Although a direct comparison between the Si/($Na_{sil.}$ + K) ratios of the two basins is hampered by lithological effects (Ma et al., 2020), the relationship observed in the Yalongjiang could indicate the transition from a kinetically limited weathering regime to an "intermediate" regime, whereas the trend we observe in the Xijiang could reflect the transition from such "intermediate" regime to supply-limited weathering regime. The Li isotopes dataset of Wang et al. (2015) for the whole Changjiang basin characterized by a large range of weathering regimes, confirms the bell-shape evolution curve of the dissolved Li isotope compositions as a function of the Si/($Na_{sil.}$ + K) ratios (Fig. SI 14), analogous to the global relationship between the riverine dissolved δ^7Li values and the ratio between the chemical weathering rates and the total denudation rates (Dellinger et al., 2015).

As all the samples of this study have been collected in zones of relatively flat topography, in addition to a change of soil weathering intensity, fractionation during the interaction between dissolved Li and sediments deposited in alluvial plains could contribute to some of the high dissolved Li isotope compositions observed across the Xijiang basin. In this view, spatial extension of the flooded areas during the wet season could allow for longer water/rock interaction within the alluvial plains, enhancing the formation of secondary minerals or the adsorption of Li onto mineral surfaces, and would contribute to the enrichment in the heavy Li isotope in river water during summer. Hence, enhanced incorporation/adsorption of Li into/onto secondary minerals formation in floodplains during the wet season could contribute to the seasonal variations of the riverine dissolved δ^7Li values observed in the Xijiang basin.

4.5. Potential impact of river management and regulation on the Li isotopic composition of suspended sediments in the Xijiang basin

One of the most striking features of our dataset is the seasonal variation of δ^7Li in the SPM (Fig. 2b). Although the δ^7Li values for both seasons follow the same evolution along the main stream, with the exception of one sample, the SPM Li isotope compositions during the wet season are systematically enriched in the light isotope relative to those collected during the dry season in the middle and lower reaches. Such seasonality in the SPM Li isotope compositions is also observed in most of the tributaries (Fig. 2b). On average, the SPM δ^7Li values during the wet season are lower by 0.5‰ compared with those of the dry season for both the main stream and tributaries.

Although in principle the evolution of the SPM Li isotopic composition along the main stream can be explained by the contribution of large tributaries, the enrichment in ^{7}Li of the main stream SPM during the dry season cannot be attributed to seasonal variations in the contributions from tributaries, as no tributary transports sediments characterized by SPM δ^7Li heavier than those observed in the main stream during the dry season.

In addition, this observation of higher SPM δ^7Li values during the dry season is counter intuitive in the perspective of hydrodynamics as one can expect that clay-rich, fine particles enriched in the light Li isotope (Dellinger et al., 2014) are more easily transported during the low-flow period (Bouchez et al., 2011a). We contend that in the Xijiang Basin the Li isotope composition of the SPM collected at the surface is representative of the entire suspended sediment load despite a potential sorting effect along the water column (Bouchez et al., 2011a, 2011b). This contention is supported by the analysis of sediments collected along depth profiles across the Xijiang main stream (Table SI 6), which show a narrow range of δ^7Li values. Hence, the observed seasonality is probably not due to a sampling bias and rather reflects seasonal changes in the sediment properties.

This seasonal pattern could be explained by an enhanced supply of relatively fine particles rich in clays (and thus displaying low Li isotopic compositions) during the wet season through accrued soil erosion, whereas during the dry season, sediments transported by the river would be derived from the erosion and resuspension of coarser sediments previously deposited on the river bed. This interpretation is partly supported by the inverse relationship between the Al/Si mass ratio used as a proxy of grain size (Bouchez et al., 2011b) and the SPM δ^7Li values (Fig. SI 15) which indicates that sediments collected during the dry season are coarser than those collected during the wet season.

Such effect of seasonality in soil erosion rate on the Li isotope signature of SPM could be reinforced by reservoir management and regulation. During the wet season, water storage in reservoirs along the main stream typically results in the retention of coarser sediment, favoring the transport of finer particles enriched in ^{6}Li whereas during the dry season, release of water from reservoirs would enhance the erosion of the river bed and banks, re-suspending coarser particles characterized by higher δ^7Li values. Concomitantly, release of water during the dry season could be accompanied with flushing of coarser particles stored in reservoirs. This interpretation is supported by the evolution of the seasonal pattern of the Xijiang water discharge since the river impoundment, characterized by a decrease of the maximum discharge during the wet season and an increase of the water discharge during the dry season, attributed to the regulation of water storages in reservoirs (Zhang et al., 2012).

However, in spite of the potential impact of river regulation on the SPM Li isotope composition, the Li isotope fingerprint of weathering is robustly archived in the sediments. This is illustrated in Fig. 8 where the δ^7Li values of the SPM collected during the wet season are plotted as a function of the weathering intensity W/D, defined here as the ratio between the silicate weathering rate W and the total denudation rate D, the sum of the silicate weathering rate and the physical erosion rate. In the absence of

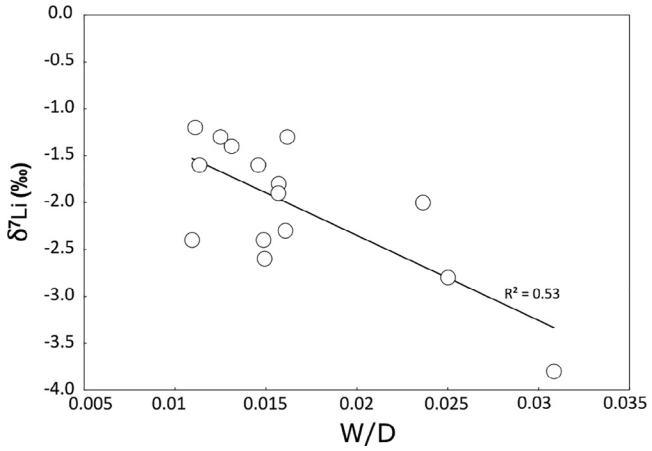

Fig. 8. Relationship between the SPM Li isotope composition for the samples collected during the wet season in the Xijiang main stream and its tributaries (squares) and the weathering intensity W/D. The weathering rates, W, are calculated by multiplying the modeled annual runoff (Döll et al., 2003) with the TDS_{sil} (total dissolved solid) derived from silicate weathering. TDS_{sil} is defined as the sum of Na_2O, K_2O, CaO, MgO and SiO_2 derived from silicate weathering. Silicon is assumed to be entirely derived from silicate weathering whereas for other elements the contributions from cyclic and anthropogenic inputs in the case of Na (see text) and carbonate in the case of Ca (see text for details) and Mg have to be taken into account. For Mg, the fraction of Mg derived from silicate weathering is calculated by subtracting the amount of Mg derived from cyclic inputs and by carbonate weathering. The fraction of Mg derived from carbonate weathering is calculated based on the estimated amount of Ca derived from carbonate and by assuming a Ca/Mg molar ratio of 7 in carbonate rocks in the range of the values reported by Han and Liu (2004). The total denudation rates, D, is the sum of W and the modeled soil erosion rates (Borrelli et al., 2017).

other data, to estimate physical erosion rates, we use modeled soil erosion rates (Borrelli et al., 2017). Although the absolute values might not correspond to the actual erosion rates, these modeled values provide a first-order indication of the relative variation in physical erosion rates across the basin. The negative SPM δ^7Li -W/D relationship is in line with observations from fine river sediments at the global scale (Dellinger et al., 2017) and consistent with the conclusion of He et al. (2020) of an eastward increase of weathering intensity based on the spatial evolution of the clay assemblage and the general increase of the relative proportion of kaolinite from the Upper Reach to the Lower Reach. Altogether, our analysis of Li isotope composition of river material in the Xijiang basin confirms the robustness of Li isotopes as a proxy of weathering and erosion processes, even in this heavily-managed river system.

5. CONCLUSIONS

In the Xijiang basin, the dissolved Li isotope composition of river waters varies between +16‰ and +27‰ and is higher values during the wet season than in the dry season. These values are much higher than the estimated the bedrock composition (~0‰), which is explained by the preferential incorporation of the light Li isotopes in secondary phases formed during the incongruent dissolution of silicate rocks. We show that the spatial variations of the dissolved δ^7Li values across the basin mainly reflect changes in silicate weathering intensity. We interpret the high Li isotope composition as a consequence of the limited supply of Li by chemical weathering. This interpretation is supported by the positive relationship between the soil erosion rates and the dissolved Li fluxes. In the mountainous part of the basin, the relatively higher weathering rates are likely to favor the production of secondary phases, such that the subsequent incorporation of Li in the secondary phases leaves a solution enriched in ^{7}Li. Conversely, in the lowlands which are characterized by lower soil erosion rates and more abundant rainfall, chemical weathering is more intense and the formation of secondary minerals limited resulting in lower dissolved δ^7Li values. The seasonal variation of the dissolved δ^7Li values could be related to the spatial extension of the flooded areas during the wet season which would allow longer interactions between water and sediments stored in the alluvial plains, enhancing the formation of secondary minerals and/or the adsorption of Li onto mineral surfaces.

The Li isotope composition of the suspended sediments of the Xijiang basin rivers are systematically lower than the composition of the bedrock. The lower Li isotopic compositions of the suspended sediment samples collected during the wet season compared to those of the samples collected during the dry season could be explained by the seasonal changes in the sediment properties, possibly related to reservoir management and regulation. In this interpretation, during the wet season, suspended sediments would be dominated by products of soil erosion, rich in clay minerals, whereas during the dry season, the suspended sediment load would be enriched in coarser particles resuspended from the river bed or flushed away when water is released from the reservoirs. Retention of coarser particles in reservoirs during the wet season and enhanced river bed/bank erosion during the dry season related to the release of water from reservoirs could explain the seasonal pattern of SPM Li isotope compositions. However, the relationship between the δ^7Li values of the SPM collected during the wet season and the weathering intensity suggest that the Li isotope fingerprint of weathering is preserved, confirming the robustness of Li isotopes as a proxy of

weathering and erosion processes even in heavily-managed river systems.

Declaration of Competing Interest

The authors declare that they have no known competing financial interests or personal relationships that could have appeared to influence the work reported in this paper.

ACKNOWLEDGMENTS

We thank the Editor, Jeffrey Catalano, the Associate Editor, Fang-Zhen Teng and three anonymous reviewers for their insightful and constructive comments which significantly improved a previous version of the manuscript.

This work was financially supported by the National Natural Science Foundation of China (NNSFC), grants 41561134017, U1612442, 41625012, the Agence Nationale de la Recherche (ANR), grant ANR-15-CE01-0012 and by Tianjin University for the visit of JB at ISESS, Tianjin University, grant T2018019.

APPENDIX A. SUPPLEMENTARY MATERIAL

Supplementary data to this article can be found online at https://doi.org/10.1016/j.gca.2021.08.015.

REFERENCES

Andrews E., Pogge von Strandmann P. A. E. and Fantle M. S. (2020) Exploring the importance of authigenic clay formation in the global Li cycle. *Geochim. Cosmochim. Acta* **289**, 47–68.

Bagard M. L., West A. J., Newman K. and Basu A. R. (2015) Lithium isotope fractionation in the Ganges-Brahmaputra floodplain and implications for groundwater impact on seawater isotopic composition. *Earth Planet. Sci. Lett.* **432**, 404–414.

Berner R. A., Lasaga A. C. and Garrels R. M. (1983) The carbonate-silicate geochemical cycle and its effect on atmospheric carbon dioxide over the past 100 million years. *Am. J. Sci.* **283**, 641–683.

Borrelli P., Robinson D. A., Fleischer L. R., Lugato E., Ballabio C., Alewell C., Meusburger K., Modugno S., Schutt B., Ferro V., Bagarello V., Oost K. V., Montanarella L. and Panagos P. (2013) An assessment of the global impact of 21st century land use change on soil erosion 2017. *Nat. Commun.* **8**(1).

Bouchez J., Lajeunesse E., Gaillardet J., France-Lanord C., Dutra-Maia P. and Maurice L. (2010) Turbulent mixing in the Amazon River: The isotopic memory of confluences. *Earth Planet. Sci. Lett.* **290**(1), 37–43.

Bouchez J., von Blanckenburg F. and Schuessler J. A. (2013) Modeling novel stable isotope ratios in the weathering zone. *Am.J.Sci.* **313**, 267–308.

Bouchez J., Gaillardet J., France-Lanord C., Maurice L. and Dutra-Maia P. (2011a) Grain size control of river suspended sediment geochemistry: Clues from Amazon River depth-profiles. *Geochem. Geophys. Geosyst.* **12**(3), 1–24.

Bouchez J., Lupker M., Gaillardet J., France-Lanord C. and Maurice L. (2011b) How important is it to integrate riverine suspended sediment chemical composition with depth? Clues from Amazon River depth-profiles. *Geochim. Cosmochim. Acta* **75**(22), 6955–6970.

Chan L. H., Edmond J. M., Thompson G. and Gillis K. (1992) Lithium isotope composition of submarine basalts: implications for the lithium cycle in the oceans. *Earth Planet. Sci. Lett.* **108**, 151–160.

Caves Rugenstein J. K., Ibarra D. E. and von Blanckenburg F. (2019) Neogene cooling driven by land surface reactivity rather than increased weathering fluxes. *Nature* **571**, 99–102.

Chan L. H., Starinskym A. and Katzm A. (2002) The behavior of lithium and its isotopes in oilfield brines: evidence from the Heletz-Kokhav field, Israel. *Geochim. Cosmochim. Acta* **66**, 615–623.

Chen J.-B., Gaillardet J. and Louvat P. (2008) Zinc isotopes in the Seine River water, France: a probe of anthropogenic contamination. *Environ. Sci. Technol.* **42**(17), 6494–6501.

Chen J.-B., Gaillardet J., Bouchez J., Louvat P. and Wang Y.-N. (2014) Anthropophile elements in river sediments: Overview from the Seine River, France. *Geochem. Geophys. Geosyst.* **15** (11), 4526–4546.

Chen J. B., Wang Z., Yuan W., Zhang T. and Cai H. (2019) Isotopic compositions reveal impacts of different weathering regimes on metals in river systems. *Goldschmidt Conference Abstract*.

Clergue C., Dellinger M., Buss H. L., Gaillardet J., Benedetti M. F. and Dessert C. (2015) Influence of atmospheric deposits and secondary minerals on Li isotopes budget in a highly weathered catchment, Guadeloupe (Lesser Antilles). *Chem. Geol.* **414**, 28–41.

Dellinger M., Bouchez J., Gaillardet J., Faure L. and Moureau J. (2017) Tracing weathering regimes using the lithium isotope composition of detrital sediments. *Geology* **45**(5), 411–414.

Dellinger M., Gaillardet J., Bouchez J., Calmels D., Galy V., Hilton R. G., Louvat P. and France-Lanord C. (2014) Lithium isotopes in large rivers reveal the cannibalistic nature of modern continental weathering and erosion. *Earth Planet. Sci. Lett.* **401**, 359–372.

Dellinger M., Gaillardet J., Bouchez J., Calmels D., Louvat P., Dosseto A., Gorge C., Alanoca L. and Maurice L. (2015) Riverine Li isotope fractionation in the Amazon River basin controlled by the weathering regimes. *Geochim. Cosmochim. Acta* **164**, 71–93.

Döll P., Kaspar F. and Lehner B. (2003) A global hydrological model for deriving water availability indicators: model tuning and validation. *J. Hydrol.* **270**(1), 105–134.

Froelich F. and Misra S. (2014) Was the late Paleocene-early Eocene hot because Earth was flat? An ocean lithium isotope view of mountain building, continental weathering, carbon dioxide, and Earth's Cenozoic climate. *Oceanography* **27**(1), 36–49.

Gaillardet J., Dupre B. and Allegre C. J. (1999a) Geochemistry of large river suspended sediments: Silicate weathering or recycling tracer? *Geochim. Cosmochim. Acta* **63**(23–24), 4037–4051.

Gaillardet J., Dupre B., Louvat P. and Allegre C. J. (1999b) Global silicate weathering and CO2 consumption rates deduced from the chemistry of large rivers. *Chem. Geol.* **159**(1–4), 3–30.

Gou L. F., Jin Z., Pogge von Strandmann P. A. E., Li G., Qu Y. X., Xiao J., Deng L. and Galy A. (2019) Li isotopes in the middle Yellow River: Seasonal variability, sources and fractionation. *Geochim. Cosmochim. Acta* **248**, 88–108.

Guinoiseau D., Bouchez J., Gelabert A., Louvat P., Filizola N. and Benedetti M. F. (2016) The geochemical filter of large river confluences. *Chem. Geol.* **441**, 191–203.

Guinoiseau D., Bouchez J., Gelabert A., Louvat P., Moreira-Turcq P., Filizola N. and Benedetti M. F. (2018) Fate of particulate copper and zinc isotopes at the Solimoes-Negro river confluence, Amazon Basin, Brazil. *Chem. Geol.* **489**, 1–15.

Han G. and Liu C.-Q. (2004) Water geochemistry controlled by carbonate dissolution: a study of the river waters draining karst-dominated terrain, Guizhou Province, China. *Chem. Geol.* **204**(1), 1–21.

Hartmann J. and Moosdorf N. (2012) The new global lithological map database GLiM: A representation of rock properties at the Earth surface. *Geochem. Geophys. Geosyst.* **13**(12).

Hathorne E. C. and James R. H. (2006) Temporal record of lithium in seawater: A tracer for silicate weathering? *Earth Planet. Sci. Lett.* **246**(3–4), 393–406.

He L., Garzanti E., Dinis P., Yang S. and Wang H. (2020) Provenance versus weathering control on sediment composition in tropical monsoonal climate (South China) -1. Geochemistry and clay mineralogy. *Chem. Geol.* **558**, 119860.

Henchiri S., Gaillardet J., Dellinger M., Bouchez J. and Spencer R. G. M. (2016) Riverine dissolved lithium isotopic signatures in low-relief central Africa and their link to weathering regimes. *Geophys. Res. Lett.* **43**(9), 4391–4399.

Hilton R. G. and West A. J. (2020) Mountains, erosion and the carbon cycle. *Nat. Rev. Earth. Environ.* **1**, 284–299.

Hindshaw R. S., Tosca R., Goût T. L., Farnan I., Tosca N. J. and Tipper E. T. (2019) Experimental constraints on Li isotope fractionation during clay formation. *Geochim. Cosmochim. Acta* **250**, 219–237.

Hu D., Clift P. D., Boning P., Hannigan R., Hillier S., Blusztajn J., Wan S. and Fuller D. Q. (2013) Holocene evolution in weathering and erosion patterns in the Pearl River delta. *Geochem. Geophys. Geosyst.* **14**(7), 2349–2368.

Hu Z. and Gao S. (2008) Upper crustal abundances of trace elements: A revision and update. *Chem. Geol.* **253**(3), 205–221.

Huh Y., Chan L. H., Zhang L. and Edmond J. M. (1998) Lithium and its isotopes in major world rivers: Implications for weathering and the oceanic budget. *Geochim. Cosmochim. Acta* **12**, 2039–2051.

Huh Y., Chan L.-H. and Edmond J. M. (2001) Lithium isotopes as a probe of weathering processes: Orinoco River. *Earth Planet. Sci. Lett.* **194**(1), 189–199.

Jiang H., Liu W., Zhao T., Sun H. and Xu Z. (2018) Water geochemistry of rivers draining karst-dominated regions, Guangxi province, South China: Implications for chemical weathering and role of sulfuric acid. *J. Asian Earth Sci.* **163**, 152–162.

Jiao S.-J., Li X.-H., Huang H.-Q. and Deng X.-G. (2015) Metasedimentary melting in the formation of charnockite: Petrological and zircon U-Pb-Hf-O isotope evidence from the Darongshan S-type granitic complex in southern China. *Lithos* **239**, 217–233.

Kisakurek B., James R. H. and Harris N. B. W. (2005) Li and δ^7Li in Himalayan rivers: Proxies for silicate weathering? *Earth Planet. Sci. Lett.* **237**(3–4), 387–401.

Kuessner M. L., Gourgiotis A., Manhes G., Bouchez J., Zhang X. and Gaillardet J. (2019) Automated analyte separation by ion chromatography using a cobot applied to geological reference materials for Li isotope composition. *Geostand. Geoanal. Res.* **44**(1), 57–67.

Lemarchand E., Chabaux F., Vigier N., Millot R. and Pierret M. C. (2010) Lithium isotope systematics in a forested granitic catchment (Strengbach, Vosges Mountains, France). *Geochim. Cosmochim. Acta* **74**(16), 4612–4628.

Li W. and Liu X.-M. (2020) Experimental investigation of lithium isotope fractionation during kaolinite adsorption: Implications for chemical weathering. *Geochim. Cosmochim. Acta* **284**, 156–172.

Li G. J. and West A. J. (2014) Evolution of Cenozoic seawater lithium isotopes: coupling of global denudation regime and shifting seawater sinks. *Earth Planet. Sci. Lett.* **401**, 284–293.

Linke S., Lehner B., Ouellet D. C., Ariwi J., Grill G., Anand M., Beames P., Burchard-Levine V., Maxwell S., Moidu H., Tan F. and Thieme M. (2019) Global hydro-environmental sub-basin and river reach characteristics at high spatial resolution. *Sci. Data* **6**, 283.

Liu M., Fan D., Bi N., Sun X. and Tian Y. (2019) Impact of water-sediment regulation on the transport of heavy metals from the Yellow River to the sea in 2015. *Sci. Total Environ.* **658**, 268–279.

Liu X.-M. and Rudnick R. L. (2011) Constraints on continental crustal mass loss via chemical weathering using lithium and its isotopes. *Proc. National Acad. Sci. U. S. A.* **108**(52), 20873–20880.

Liu X. M., Wanner C., Rudnick R. L. and McDonough W. F. (2015) Processes controlling d7Li in rivers illuminated by study of streams and groundwaters draining basalts. *Earth Planet. Sci. Lett.* **409**, 212–224.

Ma L., Qiao X., Min L., Fan B., Ding X. and Dai W. (2002) *Geological Atlas of China*. Geological Publishing House, Beijing, China.

Ma T., Weynell M., Li S.-L., Liu Y., Chetelat B., Zhong J., Xu S. and Liu C.-Q. (2020) Lithium isotope compositions of the Yangtze River headwaters: Weathering in high-relief catchments. *Geochim. Cosmochim. Acta* **280**, 46–65.

Maffre P., Godderis Y., Vigier N., Moquet J. S. and Carretier S. (2020) Modelling the riverine d7Li variability throughout the Amazon Basin. *Chem. Geol.* **532**.

Millot R., Vigier N. and Gaillardet J. (2010a) Behaviour of lithium and its isotopes during weathering in the Mackenzie Basin, Canada. *Geochim. Cosmochim. Acta* **74**(14), 3897–3912.

Millot R., Petelet-Giraud E., Guerrot C. and Negrel P. (2010b) Multi-isotopic composition (δ^7Li-δ^{11}B-δD-δ^{18}O) of rainwaters in France: Origin and spatio-temporal characterization. *Appl. Geochem.* **25**(10), 1510–1524.

Misra S. and Froelich P. N. (2012) Lithium isotope history of cenozoic seawater: Changes in silicate weathering and reverse weathering. *Science* **335**(6070), 818–823.

Murphy M. J., Porcelli D., Pogge von Strandmann P. A. E., Hirst C. A., Kutscher L., Katchinoff J. A., Morth C. M., Maximov T. and Andersson P. S. (2019) Tracing silicate weathering processes in the permafrost-dominated Lena River watershed using lithium isotopes. *Geochim. Cosmochim. Acta* **245**, 154–171.

Pearl River Water Resources Commission, http://www.pearlwater.gov.cn (in Chinese).

Penniston-Dorland S., Liu X. M. and Rudnick R. L. (2017) Lithium isotope geochemistry. *Rev. Mineral. Geochem.* **82**, 165–217.

Pistiner J. S. and Henderson G. M. (2003) Lithium-isotope fractionation during continental weathering processes. *Earth Planet. Sci. Lett.* **214**(1–2), 327–339.

Pogge von Strandmann P. A. E., Frings P. J. and Murphy M. J. (2017) Lithium isotope behaviour during weathering in the Ganges Alluvial Plain. *Geochim. Cosmochim. Acta* **198**, 17–31.

Qi L. and Zhou M.-F. (2008) Platinum-group elemental and Sr-Nd-Os isotopic geochemistry of Permian Emeishan flood basalts in Guizhou Province, SW China. *Chem. Geol.* **248**(1), 83–103.

Roy S., Gaillardet J. and Allegre A. J. (1999) Geochemistry of the dissolved and suspended loads of the Seine river, France: anthropogenic input, carbonate and silicate weathering. *Geochim. Cosmochim. Acta* **63**(9), 1277–1292.

Rudnick R. L., Tomascak P. B., Njo H. B. and Gardner L. R. (2004) Extreme lithium isotopic fractionation during continental weathering revealed in saprolites from South Carolina. *Chem. Geol.* **212**(1), 45–57.

Ryu J. S., Vigier N., Lee S. W., Lee K. S. and Chadwick O. A. (2014) Variation of lithium isotope geochemistry during basalt weathering and secondary mineral transformations in Hawaii. *Geochim. Cosmochim. Acta* **145**, 103–115.

Sauzeat L., Rudnick R. L., Chauvel C., Garcon M. and Tang M. (2015) New perspectives on the Li isotopic composition of the upper continental crust and its weathering signature. *Earth Planet. Sci. Lett.* **428**, 181–192.

Stallard R. F. and Edmond J. M. (1987) Geochemistry of the Amazon 3. Weathering chemistry and limits to dissolved inputs. *J. Geophys. Res.* **92**, 8293–8302.

Sun H., Xiao Y., Gao Y., Zhang G., Casey J. F. and Shen Y. (2018) Rapid enhancement of chemical weathering recorded by extremely light seawater isotopes at the Permian-Triassic boundary. *PNAS* **115**, 3782–3787.

Teng F. Z., McDonough W. F., Rudnick R. L., Dalpé C., Tomascak P. B., Chappell B. W. and Gao S. (2004) Lithium isotopic composition and concentration of the upper continental crust. *Geochim. Cosmochim. Acta* **68**(20), 4167–4178.

Teng F.-Z., Li W.-Y., Rudnick R. L. and Gardner L. R. (2010) Contrasting lithium and magnesium isotope fractionation during continental weathering. *Earth Planet. Sci. Lett.* **300**(1–2), 63–71.

Tomascak P. B., Magna T. and Dohmen R. (2016) The surficial realm: Low temperature geochemistry of lithium. *Adv. Isotope Geochem.*, 157–189.

Vigier N., Decarreau A., Millot R., Carignan J., Petit S. and France-Lanord C. (2008) Quantifying Li isotope fractionation during smectite formation and implications for the Li cycle. *Geochim. Cosmochim. Acta* **72**(3), 780–792.

Vigier N., Gislason S. R., Burton K. W., Millot R. and Mokadem F. (2009) The relationship between riverine lithium isotope composition and silicate weathering rates in Iceland. *Earth Planet. Sci. Lett.* **287**(3–4), 434–441.

Vigier N. and Godderis Y. (2015) A new approach for modeling the Cenozoic oceanic lithium isotope paleo-variations: the key role of climate. *Clim. Past.* **11**, 635–645.

Walker J., Hays P. and Kasting J. (1981) A negative feedback mechanism for the long-term stabilization of the Earth's surface temperature. *J. Geophys. Res.* **86**, 9776–9782.

Wang P., Yu J., Sun T., Shi Y., Chen P., Zhao K., Chen W. and Liu Q. (2013) Composition variations of the Sinian-Cambrian sedimentary rocks in Hunan and Guangxi provinces and their tectonic significance. *Sci. China Earth Sci.* **56**(11), 1899–1917.

Wang Q. L., Chetelat B., Zhao Z. Q., Ding H., Li S. L., Wang B. L., Li J. and Liu X. L. (2015) Behavior of lithium isotopes in the Changjiang River system: Sources effects and response to weathering and erosion. *Geochim. Cosmochim. Acta* **151**, 117–132.

Wang W., Zhou M.-F., Yan D.-P. and Li J.-W. (2012) Depositional age, provenance, and tectonic setting of the Neoproterozoic Sibao Group, southeastern Yangtze Block, South China. *Precambr. Res.* **192–195**, 107–124.

Weynell M., Wiechert U. and Schuessler J. A. (2017) Lithium isotopes and implications on chemical weathering in the catchment of Lake Donggi Cona, northeastern Tibetan Plateau. *Geochim. Cosmochim. Acta* **213**, 155–177.

Wimpenny J., James R. H., Burton K. W., Gannoun A., Mokadem F. and Gislason S. R. (2010) Glacial effects on weathering processes: New insights from the elemental and lithium isotopic composition of West Greenland rivers. *Earth Planet. Sci. Lett.* **290**(3–4), 427–437.

Wimpenny J., Colla C. A., Yu P., Yin Q.-Z., Rustad J. R. and Casey W. H. (2015) Lithium isotope fractionation during uptake by gibbsite. *Geochim. Cosmochim. Acta* **168**, 133–150.

Wu C. S., Yang S. L. and Lei Y.-P. (2012) Quantifying the anthropogenic and climatic impacts on water discharge and sediment load in the Pearl River (Zhujiang), China (1954–2009). *J. Hydrol.* **452–453**, 190–204.

Xiong C., Niu Y., Chen H., Chen A., Zhang C., Li F., Yang S. and Xu S. (2018) Detrital zircon U-Pb geochronology and geochemistry of late Neoproterozoic-early Cambrian sedimentary rocks in the Cathaysia Block: constraint on its palaeo-position in Gondwana supercontinent. *Geol. Mag.* **156**(9), 1587–1604.

Xu Z. and Liu C.-Q. (2007) Chemical weathering in the upper reaches of Xijiang River draining the Yunnan-Guizhou Plateau, Southwest China. *Chem. Geol.* **239**(1), 83–95.

Xu Z. and Liu C.-Q. (2010) Water geochemistry of the Xijiang basin rivers, South China: Chemical weathering and CO2 consumption. *Appl. Geochem.* **25**(10), 1603–1614.

Yang J., Cawood P. A., Du Y., Huang H. and Hu L. (2012) Detrital record of Indosinian mountain building in SW China: Provenance of the Middle Triassic turbidites in the Youjiang Basin. *Tectonophysics* **574–575**, 105–117.

Yang C., Yang S., Song J. and Vigier N. (2019) Progressive evolution of the Changjiang (Yangtze River) sediment weathering intensity since the three gorges dam operation. *J. Geophys. Res. Earth Surf.* **124**(10), 2402–2416.

Zhang L., Chan L. H. and Gieskes J. M. (1998) Lithium isotope geochemistry of pore waters from Ocean Drilling Program Sites 918 and 919, Irminger Basin. *Geochim. Cosmochim. Acta* **62**, 2347–2450.

Zhang S.-R., Lu X. X., Higgitt D. L., Chen C.-T.-A., Sun H.-G. and Han J.-T. (2007) Water chemistry of the Zhujiang (Pearl River): Natural processes and anthropogenic influences. *J. Geophys. Res. Earth Surf.* **112**(F1).

Zhang S., Lu X. X., Higgitt D. L., Chen C.-T.-A., Han J. and Sun H. (2008) Recent changes of water discharge and sediment load in the Zhujiang (Pearl River) Basin, China. *Global and Planetary Change* **60**(3), 365–380.

Zhang W., Mu S.-S., Zhang Y.-J. and Chen K.-M. (2012) Seasonal and interannual variations of flow discharge from Pearl River into sea. *Water Sci. Eng.* **5**(4), 399–409.

Zhang X., Saldi G. D., Schott J., Bouchez J., Kuessner M., Montouillout V., Henehan M. and Gaillardet J. (2021) Experimental constraints on Li isotope fractionation during the interaction between kaolinite and seawater. *Geochim. Cosmochim. Acta* **292**, 333–347.

Associate editor: Fang-Zhen Teng